POLITECNICO DI MILANO

Master's Degree in Energy Engineering

Energy Department

Modelling of a Concentrated Solar Power Plant and a Case Study: Turkey

Thesis Supervisor : Associate Professor Fabio Rinaldi

Master Graduation Thesis by : Taylan Mor

Student ID number : 872920

Academic Year 2018/2019

Contents

List of Figures

List of Tables

Abstract

In this thesis, the main Concentrated Solar Power technologies explained then some models are used from the literature for the parabolic trough power plant with thermal storage, starting from the incoming solar radiation to the power output. This combined model is used for Andasol Power Plant in Guadix/Spain. The achieved results from the model are compared with the real plant data and other simulation results, the model is validated. A brief overview of the Turkish economy and import-depended energy sector is made and solar concentrated power is proposed as a solution for the independent energy sector in Turkey. Then Karapınar/Konya is chosen for the analyses and the model is simulated for the location, the achieved output results for the hypothetical twin plant of the Andasol-1 is found to be higher than the Andasol-1. As a result, Karapınar/Konya is found to be applicable for CSP.

Abstract

In questa tesi, sono state spiegate le principali tecnologie di energia solare concentrata poi alcuni modelli sono usati dalla letteratura per la potenza parabolica del trogolo impianto con accumulo termico, a partire dalla radiazione solare in arrivo a la potenza. Questo modello combinato è utilizzato per Andasol Power Plant a Guadix/Spagna. I risultati ottenuti dal modello sono confrontati con i dati reali dell'impianto e altri risultati di simulazione, il modello è convalidato. Un breve panoramica dell'economia turca e del settore energetico dipendente dalle importazioni è fatto e il potere concentrato solare è proposto come soluzione per il settore energetico indipendente in Turchia. Quindi viene scelto Karapınar/Konya le analisi e il modello sono simulati per la posizione, l'output ottenuto i risultati per l'ipotetica pianta gemella di Andasol-1 sono risultati più alti di Andasol-1. Di conseguenza, Karapınar/Konya risulta essere applicabile per CSP.

Acknowledgements

İlk olarak ömrümün sonunda kadar örnek alacağım annem Aysun Mor'a sonsuz teşekkürlerimi sunuyorum.

Göksu'ya bu süreçte verdiği tüm destekler ve tezime ettiği yardımlar için teşekkürlerimi sunuyorum.

Bu süreçte yanımda olan kardeşime, babama, tüm aileme ve arkadaşlarıma teşekkürlerimi sunuyorum.

I would like to thank to my supervisor Professor Fabio Rinaldi for his mental and educative support.

1 Introduction

1.1 Brief Overview of the Current Situation of CSP

Is it true that the world is lack of energy or world is lack of fossil fuels. Annual average of direct horizontal radiation is 170 W/m^2 when the value is yearly integrated, it is 5.4 GJ and equal to the energy that can be extracted from one barrel of oil, 200 kg of coal or 140 $m^3$of natural gas [1]. As stated in an article in Forbes total world energy consumption in 2015 was 13,000 MTOE, which can be thought of as continuous consumption of 17.4 TW, moreover this power can be supplied only by 1% of The Great Saharan Desert.[1] As can be seen in even daily newspapers, world renewable energy can be enough to supply the total demand with appropriate investments.

In this thesis, we will focus on solar concentrated power, where it stands very low with respect to other renewable sources at 4.8 GW total nominal capacity [2]. Where global installed PV capacity is 400 GW [2] and is expected to grow up to 580 GW by the end of 2018.

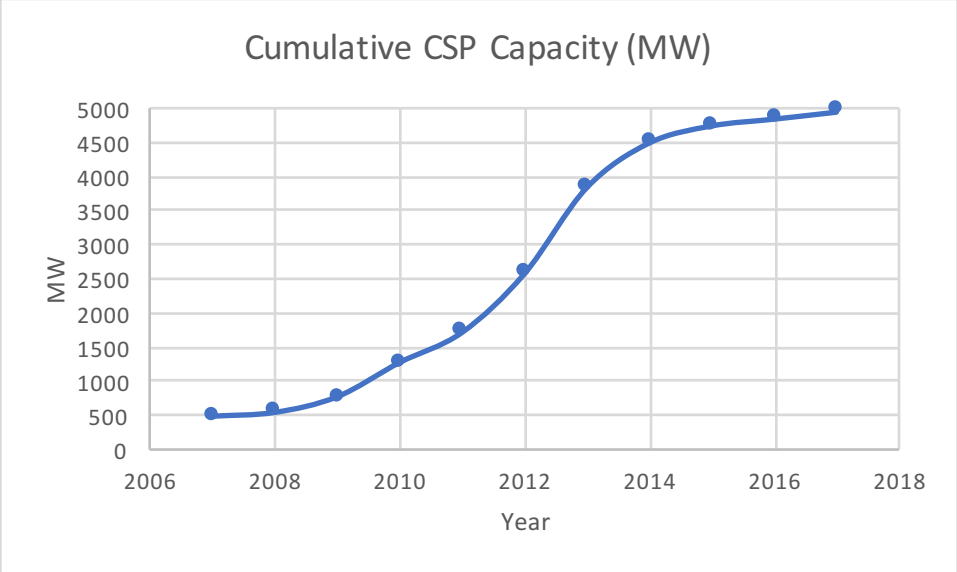

Figure 1: CSP Cumulative Capacity

Figure 1 shows the cumulative capacity addition of Concentrated Solar Power (CSP)

[1]https://www.forbes.com/sites/quora/2016/09/22/we-could-power-the-entire-world-by-harnessing-solar-energy-from-1-of-the-sahara/#f7b49e3d4406

[2]https://www.iea.org/topics/renewables/solar/

globally, in 2017 it reached 4,951 MW data is made publicly available by IRENA[3]. However, current turn out to blind to CSP technology will not last lon. On the report by IEA, by 2050 CSP supply of electricity will reach 11.3% of total supply [3] .

The main difference of CSP from PV is that CSP has the capacity to store thermal energy, which results in dispatching on cloudy days and even after sunset. Another difference is that basically CSP operates with Direct Normal Irradiance (DNI), the advantage of PV in that case, is that it can operate both with DNI and diffuse irradiance. Hence it can be said that CSP can provide reliable due to thermal storage and clean energy due to low emissions, to grid on demand. Hybridized production with CSP with other renewables is also creating an alternative for more stable dispatch to grid considering the fluctuations caused by wind and PV. Moreover CSP can be hybridized by fossil fuels.

In various sources, it is stated that CSP holds a minimum threshold around 1800 $kWh/m^2/year$ and the solar resources map below shows the possible areas for CSP technology.

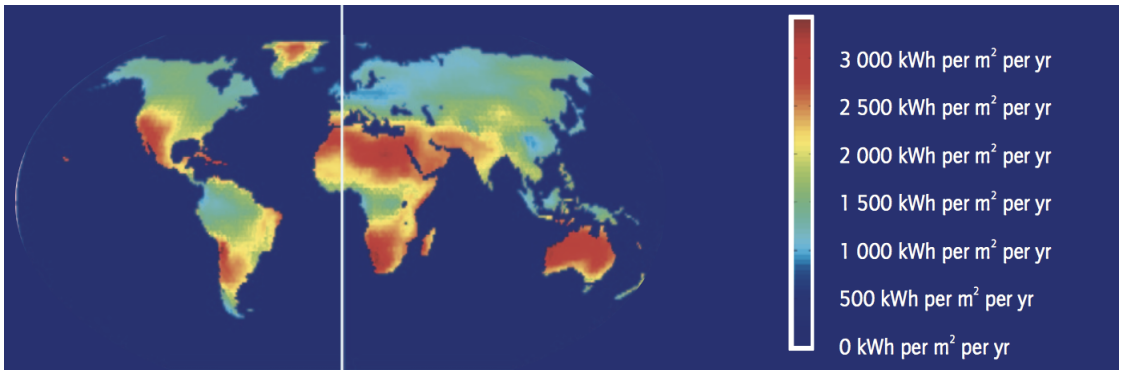

Figure 2: Solar Resource Map

Current leaders of CSP technology [2]:

- Spain with 2,362 MW
- USA with 1,804 MW
- India with 453 MW

[3]https://www.irena.org/solar

and others share smaller percentages. If we analyze the map those three countries especially India and USA are located in perfect zones for CSP, Spain with having much lower area with respect to followings but uses its resources efficiently and holds the leadership

1.2 CSP Technologies

There are various types of concentration of solar irradiation possible however there are four main technology present in commercial, and these four are sub-divided into two as :

- Linear Focus
- Point Focus

Point focus system, as can be understood from the name focuses the irradiation to receiver as a point; however linear focus systems focuses linearly to receiver and reflectors lies along the length of receiver. This results in a higher concentration ratio, higher yearly average optical efficiency in point focus systems.

1.2.1 Point Focus Systems

Figure 3: 10kW Solar Dish by Eurodish [5]

Parabolic Dishes Parabolic dishes have paraboloidal mirrors which focuses the solar energy into its receiver. Through receiver, heat is absorbed by the engine operating. Parabolic dishes have a bi-axial tracking system to keep the sun at the optical axis. Among all CSP technology Parabolic Dishes have the highest concentration ratio 1,500 to 4,000 and highest overall efficiency, converting direct normal solar irradiation into electricity reaches 30% [4]. General application of converting thermal energy into electricity is achieved by a Stirling Engine with a generator coupled since heat is supplied from outside in Stirling Engines unlike Diesel or Otto Engines where internal combustion is the source of energy.

Solar Towers Solar Tower system is also known as Central receiver consists of small heliostats (reflector mirrors) which are tracking the sun bi-axially and reflect the solar irradiation onto the fixed receiver and the concentrated thermal energy is then received by the heat transfer fluid. Than thermal energy gained by heat transfer fluid is transferred to the working fluid of the power cycle. The concentration ratio of the Solar

Tower reaches to 1000 and heat transfer fluid temperature to 1000 °C, high operating temperature results in high conversion efficiency up to 28% [6]. There are variety of receivers on the commercial market, and various types of receivers, tubular receivers of cavity type, external receiver type or volumetric receiver type. Water, air or molten salt can be used as heat transfer fluid. Water is used for direct application also in Power Block, Molten Salt usage comes with an ease of thermal storage and air in volumetric type receiver which may reach 1000 °C.

Figure 4: Crescent Dunes [7]

Crescent Dunes Power Station is located in Tonopah, Nevada and it sets a benchmark of Solar Tower type plants. This plant is the first one which commercially uses molten-salt as heat transfer fluid in Solar Tower technology. Uses external receiver type receiver and has 10 hours of storage capacity. As can be seen in Figure 4 one side which is the Northern side of tower has more heliostats than the Southern side, this is due minimizing the angle between the sunray and reflected rays [7].

1.2.2 Linear Focus Systems

Linear Fresnel Linear Fresnel technology takes its name from a French man who found the lenses for use in lighthouses in the 18th century. The first prototype of Linear Fresnel technology is built in Italy in 1964 by Giovanni Francia [8].

Figure 5: Puerto Errado-2 [9]

As can be seen in Figure 5 optical elements exists as segments. The aim is to mimic the parabolic trough reflector. In Linear Fresnel Technology reflectors made up of linear flat mirrors. The aim is to mimic as told; however fully mimicking is not possible in parabolic trough incidence angle is only affected by transversal direction but Linear Fresnel Technology is affected also from the longitudinal direction. One of the other main difference from Parabolic Trough technology is that above absorber tube there is another concentrator. This is placed for decreasing inaccuracy of Linear Fresnel since the focal is at infinite so fully concentration of rays onto fixed absorber tube is not possible, by this insulation is also achieved so the need for vacuum tube is eliminated and higher concentration ratios are present.

Linear Fresnel is capable of one axis tracking system installation, orientation of solar field can be North-South or East-West oriented. In North-South oriented plants the daily motion of the sun is tracked and this result in more annual output and East-West results in more homogenous distribution over year. In Linear Fresnel Technology water is mainly used as heat transfer fluid, so it is used directly in Power Block, direct steam generation is possible; however this creates a problem for storage capability.

Parabolic Trough The highest share of Concentrated Solar Power technology is constituted by Parabolic Trough technology. Parabolic Trough technology is somewhat similar to Linear Fresnel with some differences, Linear Fresnel mimics the parabolic

mirror; however in this case used reflector is Parabolic shaped, therefore better optical accuracy is achieved since the parabola has a focal point.

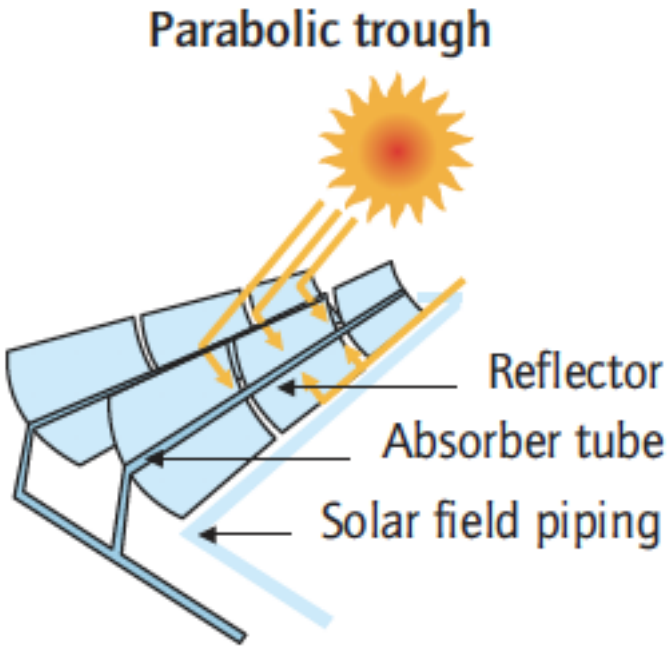

Figure 6: A Parabolic Trough Assembly

Parabolic Trough directs sunrays onto receiver with a linear manner as in Linear Fresnel, so concentration ratios are lower with respect to Point Focus systems. In Linear Focus case Parabolic Trough has the smallest concentration ratio due to limited aperture can be achieved, absorber tube is not fixed as it is in Linear Fresnel. A heat transfer fluid, in all commercial cases it is a type of synthetic oil, absorbs the thermal power and through a heat exchanger steam is generated and steam power plant is operated. Storage can be done directly by heat transfer fluid or indirectly by other fluids generally by molten salts, so another heat exchanger is used.

In this thesis, Parabolic Trough Type power plant "Andasol-1" is examined, modelled and by validated model a case study is done in a location in Turkey for an operation of the hypothetical twin power plant of "Andasol-1".

2 Modelling a Parabolic Trough Type CSP Plant

2.1 Modelling the Hourly Radiation

Solar Radiation can be divided into two: Beam Radiation and Diffuse Radiation, beam radiation is the radiation from the sun without being scattered from the atmosphere it is direct radiation from the sun. Diffuse radiation is the radiation which is scattered by the atmosphere and then received. In Concentrated Radiation applications such as CSP or CPV, the considered one is direct radiation.

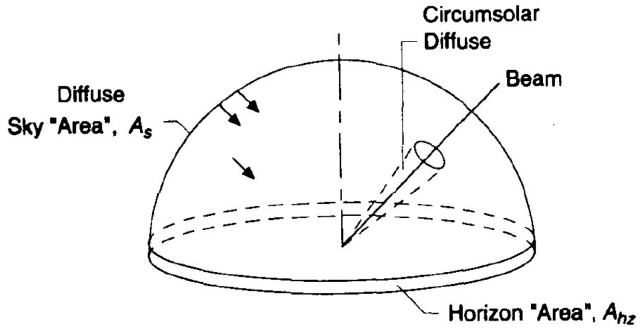

Figure 7: Diffuse and Beam components of Solar Radiation [10]

First of all to model the power plant, the necessary data is hourly radiation data in the location. Where the data is taken as Typical Meteorological Year (TMY) data for the exact coordinates of the power plant, which will be explained in detail in further sections.

In sun-angle relationships, solar time is used so the first step to model is to convert standard time in the location in solar time [10]:

$$Solar\,time - standard\,time = 4\,(L_{st} - L_{loc}) + E) \qquad (2.1.1)$$

L_{st} is the standard meridian for the local time zone,

L_{loc} is the local meridian,

$$E = 229.2\,(0.000075 + 0.001868\,cos(B) - 0.032077\,sin(B) - 0.014615\,cos(2B) - 0.04089\,sin(2B)) \qquad (2.1.2)$$

E is the equation of time in minutes and correlated with the day number of the year,

$$B = (n-1)\,\frac{360}{365} \qquad (2.1.3)$$

n is the day number of the year.

By calculating the solar time next step is to calculate the angles, to reach the incidence angle :

$$\delta = 23.45\,sin(360\,\frac{284+n}{365}) \qquad (2.1.4)$$

δ is the declination angle which is determined by the day number,

$$cos(\theta_z) = cos(\varphi)\,cos(\delta)\,cos(\omega) + sin(\varphi)\,sin(\delta) \qquad (2.1.5)$$

$\theta_z$is the zenith angle; the angle between the line to the sun and vertical line

φ is the latitude; angular location of the location according to the equator

ω is the solar hour angle

$$\omega = (solar\,time - 12)\cdot 15 \qquad (2.1.6)$$

θ is the angle of incidence; the angle which direct radiation hits the surface with

The collectors in our case will be north-south axis tracking with continuous adjustment so that ;

$$cos(\theta) = (cos^2(\theta_z) + cos^2(\delta)\,sin^2(\omega))^{0.5} \qquad (2.1.7)$$

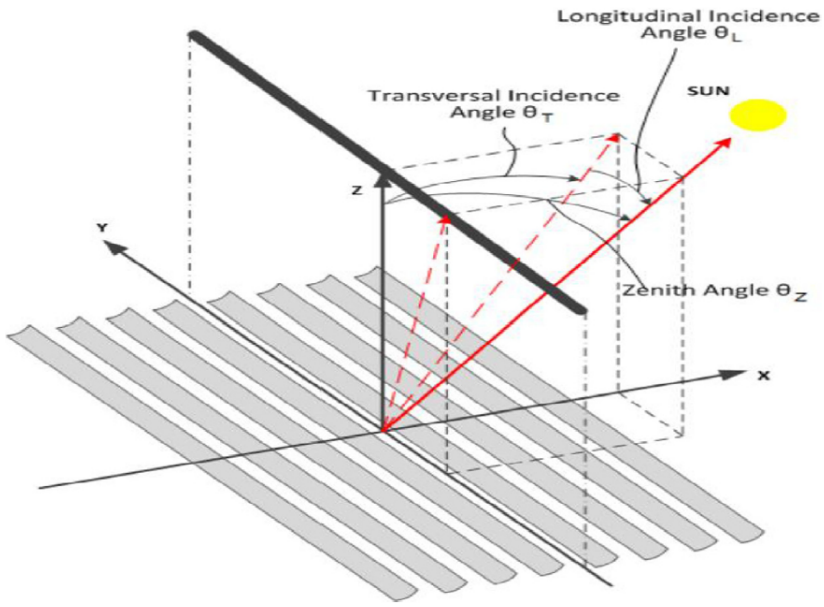

Figure 8: Incidence Angle and Zenith Angle [11]

Up to now, we are able to model the incidence angle on reflecting surface with respect to time.

$$I_{on\,surface} = I_{direct\,beam} \cdot cos(\theta)\ W/m^2 \qquad (2.1.8)$$

2.2 Modelling the Absorbed Radiation by Receiver

The hourly radiation on north-south axis tracking system is shown above, now we will move on with modelling the absorbed radiation by receiver tubes.

First to define some efficiency indexes :

Optical efficiency: It is the ratio of the direct radiation on the surface of the collector (on aperture area) and direct radiation on the absorber tube [12].

$$\eta_{optical} = \frac{E_{reciever}}{E_{on\,surface}} \qquad (2.2.1)$$

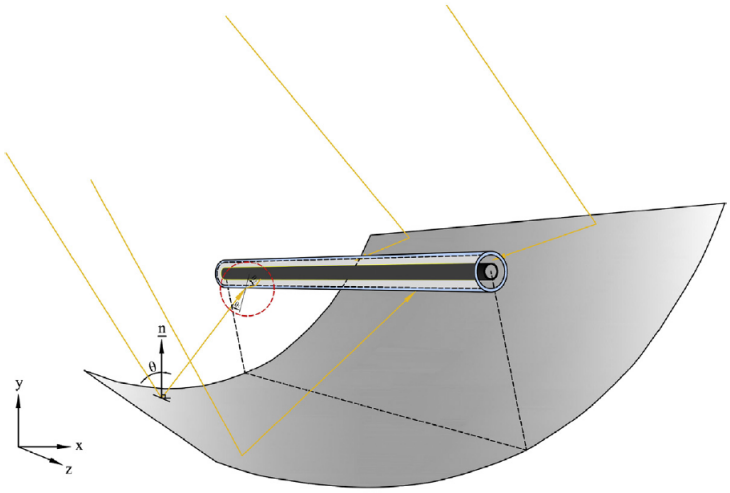

Figure 9: Beam Radiation on Receiver Tube

Factors that affect optical efficiency [13]:

- Reflectance: Parabolic Trough Collector is set of mirrors on a parabolic structure to concentrate the irradiation on to the absorber tube.
- The transmittance of cover on absorber tube: Beam Radiation has to pass through the cover.
- The absorptivity of absorber: Beam radiation has to be absorbed by the absorber.

  These are direct optical properties which affects the efficiency; however, there are further decreases in optical efficiency due to :

- Tracking error
- Fouling on mirror
- Incidence angle modifier (IAM)

  IAM is a factor that modifies the optical efficiency with respect to the nominal value of the optical efficiency

Thermal efficiency: It is the ratio of the available energy on the receiver and the absorbed value by the fluid in pipes [12]

$$\eta_{thermal} = 1 - \frac{E_{thermal\,loss}}{E_{receiver}} \qquad (2.2.1)$$

As we can see from the above formula, modelling the thermal loss from the pipe will result in reaching the useful heat gained by the heat transfer fluid.

Irradiation hits on the surface of the collector than from collector portion of it reflected to the absorber pipes heat transfer mechanism continues as:

1. Radiation reflected part hits the cover of the absorber pipe and refracted part hits the absorber pipe surface
2. Absorber tube's wall temperature increases
3. Conduction starts from the outer wall of absorber tube to inner wall
4. Fluid is flowing inside the tube and by forced convection in a tube fluid gains energy and the remaining energy is lost

The heat loss from receiver tube is due to the radial temperature difference, to model the heat loss to reach useful gained energy Yılmaz and Söyletmez developed the following mathematical model [13];

The governing energy balance equations are :

$$\dot{q}_{conv,HTF} = \dot{q}_{cond,a} \qquad (2.2.2)$$

$$\dot{q}_{cond,a} = \dot{q}_{conv,an} + \dot{q}_{rad,an} + \dot{q}_{cond,r} \qquad (2.2.3)$$

$$\dot{q}_{cond,c} = \dot{q}_{conv,air} + \dot{q}_{rad,r-s} + \dot{q}_{conv,r} + \dot{q}_{rad,r} \qquad (2.2.4)$$

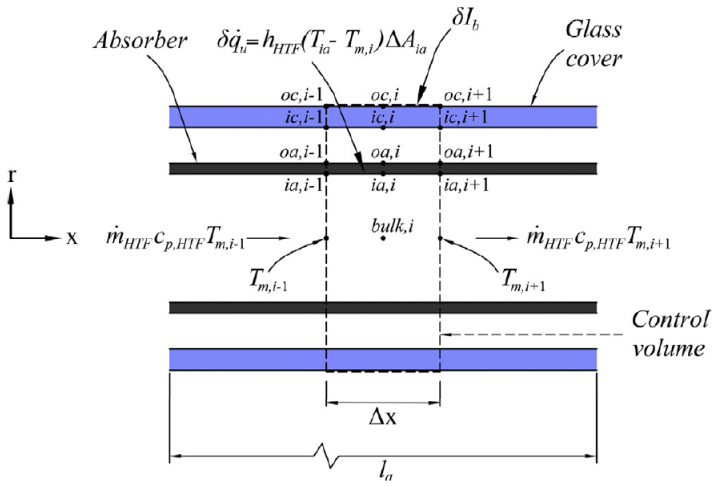

Figure 10: Heat transfer mechanism in the absorber tube [13]

Radiative flux is assumed to be constant along the tube, so mean fluid temperature increasing linearly along the tube also wall temperature increases linearly since the convection coefficient h_{htf} assumed to be constant.

Resistance Network of the absorber tube :

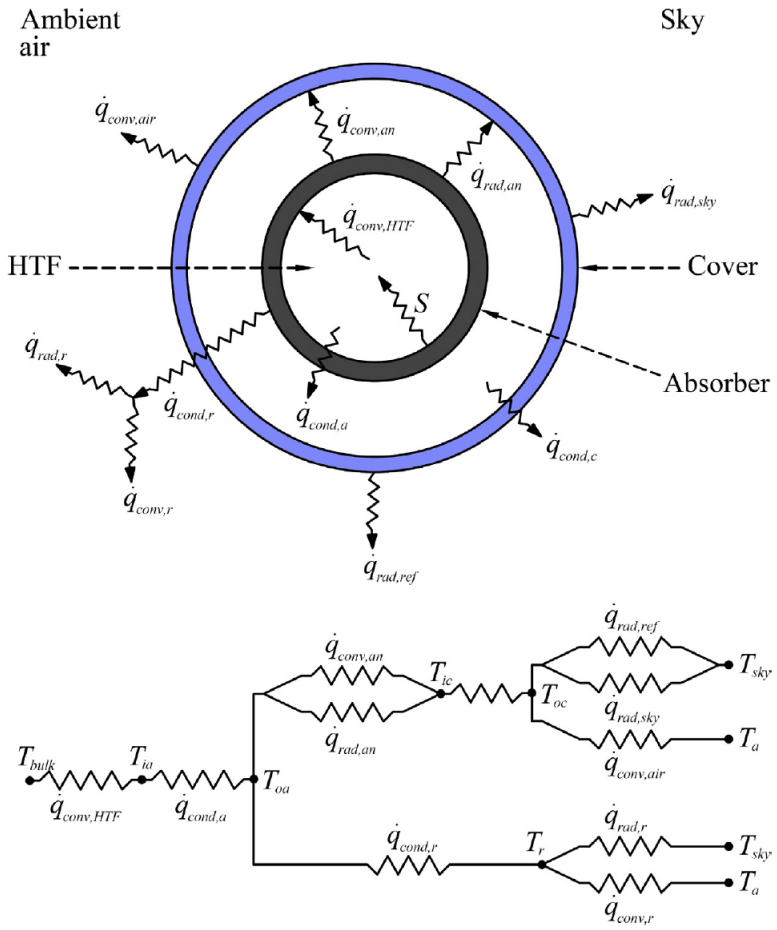

Figure 11: Resistance Network [13]

Starting from the fluid inside the tube, in flows in pipes Reynolds number is the describing number for the flow if it is laminar or turbulent [14] ,

$$Re_D \equiv \frac{\rho\, u_m\, D}{\mu} \qquad (2.2.5)$$

[14]

Where ρ, u_m, D, μ stands for density the of the fluid, mean fluid velocity, the inner diameter of the pipe and viscosity of the fluid.

Flow is considered to be laminar if [14];

$$Re_D \leq 2300 \qquad (2.2.6)$$

Flow is considered to be fully turbulent if [14];

$$Re_D \approx 10,000 \qquad (2.2.7)$$

By reaching Nusselts number we can reach the convection coefficient [14]:

$$Nu \equiv \frac{hD}{k} \qquad (2.2.8)$$

Where h, D, k stands for convection coefficient, diameter and thermal conductivity.

Since Radiation along the receiver tube is constant we can assume the convection under constant surface heat flux. For laminar flows under constant heat flux, Nusselt number is :

$$Nu = 4.364 \qquad (2.2.9)$$

And when the flow is turbulent in smooth pipes Nusselt number is [13]:

$$Nu = \frac{\sqrt{f/8}\, Re\, Pr}{12.48\, Pr^{2/3} - 7.853\, Pr^{1/3} + 3.613 ln(Pr) + 5.8 + 2.78 ln(\sqrt{f/8}\, Re\, /90)} \qquad (2.2.10)$$

The above correlation is applicable in conditions; $0.5 \leq Pr \leq 2000$and $10^4 \leq Re \leq 5 \times 10^6$and Pr, Prandtl

$$Pr \equiv \frac{v}{\alpha} \qquad (2.2.11)$$

v stands for kinematic viscosity and α stands for thermal diffusivity.

By definiton $Nu \equiv \frac{hD}{k}$ hence reaching the Nusselt number from 2.9 and 2.10 we can reach convection coefficient h.

Using Newton's law of cooling ;

$$\dot{q}_{conv,HTF} = h\, p_{ia}\, (T_{ia} - T_{bulk}) \qquad (2.2.12)$$

p_{ia} stands for the inner perimeter of absorber tube.

T_{bulk} is the mean fluid temperature of each Dx at Figure 10.

T_{ia} is the inner surface temperature of the tube.

T_{oa} is the outer surface temperature of the tube.

The left-hand side of governing equation 2.2.2 is at equation 2.2.12 and right-hand side is conduction through the absorber wall.

$$q_{cond,a} = \frac{2\,\pi\, k_a}{ln(\frac{D_{oa}}{D_{ia}})}(T_{oa} - T_{ia}) \qquad (2.2.13)$$

D_{oa} stands for outer tube's outer diameter, D_{ia} stands for tubes inner diameter, k_a is the wall conductivity, T_{oa} is the outer surface temperature of the tube.

Now we have to move on with the annulus region, the annulus region is vacuumed; however 1 torr of pressure assumption is quite reasonable in annulus and with that natural convection calculations become available. In natural convection case, Rayleigh number is used to reach Nusselt number [13].

$$Ra = \frac{g\,\beta\,(T_{oa} - T_{ic})\,L^3}{v\,\alpha} \qquad (2.2.14)$$

g is the gravitational acceleration.

T_{ic} is the inner cover temperature.

β is 1 over film temperature.

$$Nu_{an} = (Nu_{cond}^{15} + Nu_{conv}^{15})^{1/15} \qquad (2.2.15)$$

$$Nu_{cond} = \frac{2}{ln(D_{ic}/D_{ia})} \qquad (2.2.16)$$

D_{ic} is the inner cover diameter.

D_{ia} is the inner absorber tube diameter.

$$Nu_{conv} = \frac{2}{ln(\frac{1+2/Nu_i}{1-2/Nu_o})} \qquad (2.2.17)$$

$$Nu_i = 0.3987\, Ra_{an}^{1/4} \qquad (2.2.18)$$

$$Nu_o = (39.24 + (\frac{D_{ic}}{D_{ia}})^{5/4}\, Ra_{an}^{5/12})^{3/5} \qquad (2.2.19)$$

We can reach h_{an} from Nu_{an} and than by Newton's law of cooling ;

$$\dot{q}_{conv,an} = h_{an}\, p_{oa}\, (T_{oa} - T_{ic}) \qquad (2.2.20)$$

h_{an} is the convection coefficient in the annulus region.

p_{oa} is the outer perimeter of absorber tube.

Moreover, there is radiation mode heat transfer in the annulus between absorber tube and cover, since the heat transfer rate is really small we can not neglect the radiation term. The cover is assumed to be diffuse since emissivity remains constant when the incidence angle is smaller than 40° and there is continuous tracking, gray in the solar spectrum and opaque.

$$\dot{q}_{rad,a} = \frac{\sigma\, (T_{oa}^4 - T_{ic}^4)}{\frac{1-\varepsilon_a}{\varepsilon_a} + \frac{1}{F_{ac}} + \frac{1-\varepsilon_c}{\varepsilon_c}(\frac{D_{oa}}{D_{ic}})} \qquad (2.2.21)$$

σ is Stefan-Boltzman constant.

ε_a is emissivity of absorber tube.

$F_{ac}$is view factor of absorber tube to cover.

ε_c is emissivity of cover.

There are retainers in HCE where it is connecting absorber tube and cover and it is connected by support brackets to hold the tube at its position. There occurs heat transfer by conduction to the retainers and it dissipates by radiation and convection.

Support brackets are treated as fins:

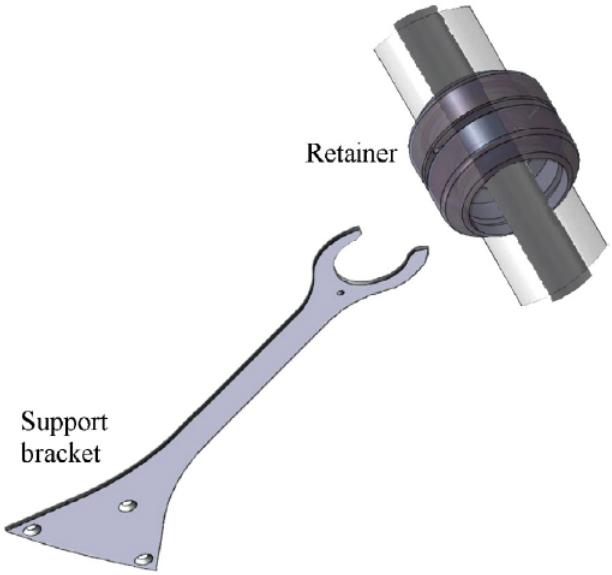

Figure 12: Support bracket and Retainer [13]

$$\dot{q}_{conv,r} = \sqrt{h_{air}\, p_r\, k_r\, A_r}(T_b - T_a)\, tanh(mL/L) \qquad (2.2.22)$$

$$q_{rad,r} = \sigma\, \varepsilon_r\, p_r\, (T_r^4 - T_{sky}^4) \qquad (2.2.23)$$

$$m = \sqrt{h_{air} p_r / k_r A_r} \qquad (2.2.24)$$

p_r is outer the perimeter of the retainer.

L is the length of the retainer.

A_r is the cross-section.

h_{air} is air convection coefficient

T_r is the temperature of the retainer.

T_b is the fin base temperature.

T_{sky} is the temperature of sky.

$$T_{sky} = 0.05532\, T_a \qquad (2.2.25)$$

k_r is thermal conductivity of the retainer.

ε_r is the emissivity of the retainer.

Radiation absorption in the cover tube is not included in the mathematical model since the absorption coefficient is really small; however, conduction is present.

$$q_{cond,c} = \frac{2\pi k_c}{ln(D_{oc}/D_{ic})}(T_{ic} - T_{oc}) \qquad (2.2.26)$$

D_{oc} is the outer cover diameter.

k_c is the thermal conductivity of cover.

T_{oc} is the outer cover temperature.

The model starts from the inside of the absorber tube and moves radially outward, and finally, we arrived to the outer section of the cover. There occur radiation and convection to ambient.

Convection from receiver to ambient, as proposed in the model, receiver orientation with respect to the wind flow direction is effective when the flow is in mixed convection

regime, this is the regime when natural and forced convection occurs together, orientation is effective when $Re > 4.5 \times 10^5$, and it is not effective when Re smaller than the value [13].

$$Nu^T = 0.772\, Ra_{air}^{1/4} \qquad (2.2.27)$$

$$Nu_l = \frac{2f}{ln(1 + 2f/Nu^T)} \qquad (2.2.28)$$

$$f = 1 - \frac{0.13}{(Nu^T)^{0.16}} \qquad (2.2.29)$$

$$Nu_t = 0.103\, Ra_{air}^{1/3} \qquad (2.2.30)$$

$$Nu_N = ((Nu_l)^{10} + (Nu_t)^{10})^{1/10} \qquad (2.2.31)$$

Re Range	9×10^{-2} to 1.0	1.0 to 35	35 to 5×10^3	5×10^3 to 5×10^4	5×10^4 to 2×10^5
a	0.800	0.795	0.583	0.148	0.0208
n	0.280	0.384	0.471	0.633	0.814

Table 1: Constants for equation 2.2.31

$$Nu_F = a\, Re^n \qquad (2.2.32)$$

where $Nu_N = Nu_F$

$$Re_i = (Nu_N/a)^{1/n} \qquad (2.2.33)$$

Then finding the effective Reynolds number,

$$Re_{eff} = ((Re_i + Re_{air}cos(\phi))^2 + (Re_{air}sin(\phi))^2)^{1/2} \qquad (2.2.34)$$

$$Nu_{air} = a\, Re_{eff}^n \qquad (2.2.35)$$

Convection coefficient can be calculated from equation 2.2.8. From Newton's law of cooling;

$$\dot{q}_{conv,air} = h_{air} p_{oc} (T_{oc} - T_a) \qquad (2.2.36)$$

Finally, there is radiation leaving the outer surface of the cover to the sky and some part is to the reflector. In the model, surface assumed as opaque, gray and diffuse. The sky is assumed to be black body radiating at T_{sky}, Reflector temperature is assumed to be T_{amb}.

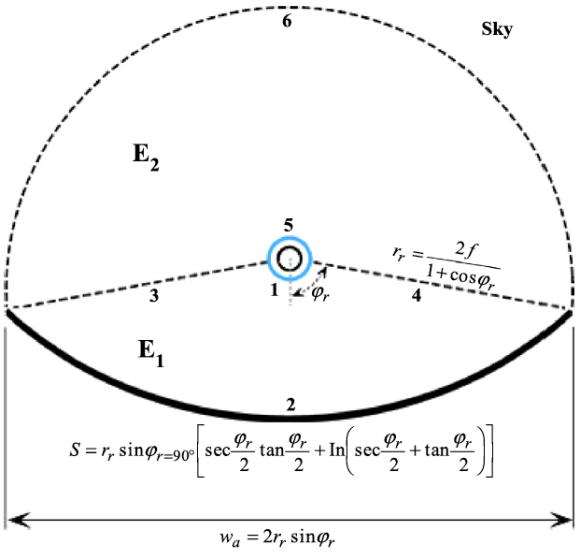

Figure 13: Surfaces [13]

$$\dot{q}_{rad,r-s} = \dot{q}_{rad,ref} + \dot{q}_{rad,sky} \qquad (2.2.36)$$

$$\dot{q}_{rad,ref} = p_1(F_{12}(J_1 - J_2) + F_{13}(J_1 - J_3) + F_{14}(J_1 - J_4)) \qquad (2.2.37)$$

$$\dot{q}_{rad,sky} = p_5(F_{56}(J_5 - J_6) + F_{53}(J_5 - J_3) + F_{54}(J_5 - J_4)) \qquad (2.2.38)$$

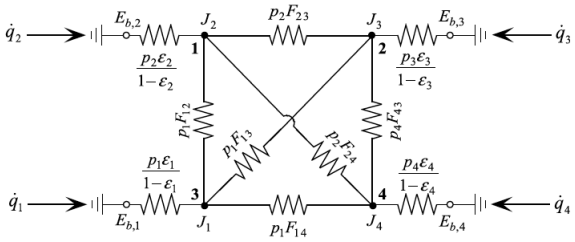

Figure 14: Radiation Network for the Cover Surface [13]

J's are radiosities and F's are view factors, equation 2.2.37 defines radiation from cover's surface 1 to reflector and equation 2.2.38 defines to the sky. View factor relations of surfaces are below [13]:

$$F_{13} = F_{14} \qquad F_{53} = F_{54} \qquad F_{23} = F_{24} \qquad (2.2.39)$$

$$F_{22} = 1 - \frac{2}{\pi} \qquad (2.2.40)$$

Now all losses are analyzed separately, the model continues with combining them into U_L named as loss factor.

$$U_L = (\frac{1}{h_{an} + h_{ac}} + \frac{1}{h_{air} + h_{c,sky}}(\frac{D_{oa}}{D_{oc}}))^{-1} \qquad (2.2.41)$$

Although h_{ac} and $h_{c,sky}$ are not convection coefficients but related to radiation, they are normalized with Temperature in order to write the loss in one single factor. Useful heat gain is calculated by every single segment in absorber tube as in Figure 10.

$$F_R = \frac{\dot{m}_{HTF} c_{p,HTF} (T_{m,i+1} - T_{m,i-1})}{w_a (S - U_L (T_{m,i-1} - T_a))} \qquad (2.2.42)$$

F_R is heat removal factor.

S is the absorbed solar energy by the receiver, $E_{reciever}$ on equation 2.2.1, direct irradiation decreased by the optical efficiency.

w_a is the aperture area.

$$\dot{q}_{useful} = F_R w_a (S - \frac{U_L}{CR} (T_{m,i-1} - T_a)) \qquad (2.2.43)$$

CR is the concentration ratio.

Model ends here, segment width should be defined and than this should be simulated until the end of absorber tube from the entrance, this model is validated with various experimental results.

Moreover, in literature there are some experimental analysis of heat loss correlations from receiver tube, Now we will introduce the model developed by National Renewable Energy Laboratory, US. They tested 2 identical Schott 2008 PTR70, from 100 °C to 500 °C to figure out the heat loss between that operating ranges. The model of Burkholder and Kutscher explained below [15].

Figure 15: NREL Test Assembly [15]

NREL set their test stand indoors, heated the absorber tubes surface by electric resistance heaters up to the desired temperature and when the desired temperature is reached electrical power required to keep the surface at constant temperature is measured. Heat Collector Elements (HCE) length is 4.06 m with absorber tubes inner diameter 6.6 cm and outer diameter 7.0 cm.

To heat the absorber tube, each of them 2.17 m long and 5.14 cm outer diameter copper pipes are inserted into the HCE from each end. Pipes are from copper tube since its thermal resistance is quite low and results in even distribution of temperature. Two of the heater inside the copper tube is 3 cm long coiled heater made up of stainless steel and the other heater is catridge heater 2.12 m long which lies in the whole lenght of the copper tube.

Figure 16: Copper Heater Tubes [15]

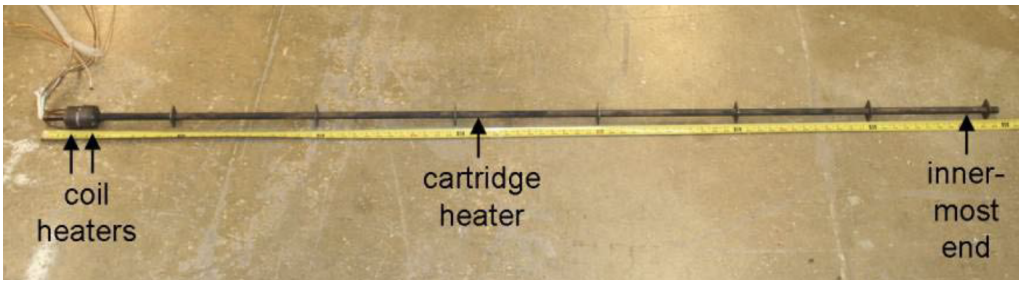

Figure 17: Heaters in Copper Tube [15]

2008 PTR70 #1

Test	**Average absorber temperature (°C)**	Average glass temperature (°C)	Average ambient temperature (°C)	Average absorber temp. above ambient (°C)	**Heat loss (W/m HCE length)**	date of test
1	**100**	26	23	77	**15**	10/13/2008
2	**153**	30	23	130	**23**	10/13/2008
3	**213**	35	23	190	**43**	10/9/2008
4	**246**	38	23	222	**59**	10/14/2008
5	**317**	50	24	293	**113**	10/9/2008
6	**346**	55	24	323	**141**	10/14/2008
7	**390**	65	24	366	**204**	10/14/2008
8	**418**	73	24	393	**257**	10/9/2008
9	**453**	82	24	430	**333**	10/14/2008
10	**458**	84	24	434	**348**	10/9/2008
11	**506**	99	24	482	**495**	10/9/2008

2008 PTR70 #2

Test	**Average absorber temperature (°C)**	Average glass temperature (°C)	Average ambient temperature (°C)	Average absorber temp. above ambient (°C)	**Heat loss (W/m HCE length)**	date of test
1	**120**	27	22	98	**15**	11/5/2008
2	**203**	33	22	180	**36**	11/5/2008
3	**254**	39	23	231	**63**	11/5/2008
4	**292**	45	23	269	**90**	11/6/2008
5	**343**	54	23	320	**140**	11/6/2008
6	**403**	68	23	380	**231**	11/6/2008
7	**404**	67	22	382	**230**	11/7/2008
8	**451**	80	23	429	**334**	11/7/2008
9	**501**	95	23	478	**481**	11/7/2008

Figure 18: Test Results of NREL

The above heat loss results are achieved by NREL with the uncertainty of $\pm 10\,W/m$, most of the solar power plants thermal fluid enters at 290 °C and leaves at 390 °C, average temperature of the fluid is 340 °C and the temperature difference between the absorber tubes outer surface to the thermal fluid can be assumed 10 °C, so average absorber surface temperature is 350 °C and the average heat loss per unit meter of absorber tube can be said as $150\,W/m$ according to test results.

Price developed the correlation in "A Parabolic Trough Solar Power Plant Simulation Model" in January 2003 [15]:

$$HL = A0 + A1(T_{HTF} - T_{amb}) + A2 \cdot T_{HTF}^2 + A3 \cdot T_{HTF}^3 + A4 \cdot I_b IAMCosTh \cdot T_{HTF}^2 ...$$

$$+\sqrt{V_w} \cdot (A5 + A6 \cdot (T_{HTF} - T_{amb})) \qquad (2.2.44)$$

T_{HTF} is the temperature of heat transfer fluid.

T_{amb} is the ambient temperature.

V_w is the wind speed.

$I_b IAMCosTh$ is the Solar Irradiation that can reach absorber tube, direct radiation times cosine of incidence angle.

HL is the heat loss in Watts per unit meter (W/m).

Burkholder and Kutscher used this correlation and found the coefficients according to their test results.

$A0$	4.05
$A1$	0.247
$A2$	-0.00146
$A3$	5.64×10^{-6}
$A4$	7.62×10^{-8}
$A5$	-1.70
$A6$	0.0125

Table 2: Heat Loss Coefficients

The correlation given at 2.43 is the heat loss in HCE per length and by using this one can estimate the solar field performance:

$$Q_{sol,abs} = I_b cos(\theta)\, Ap\, \eta_{opt}\, IAM \qquad (2.2.44)$$

Absorbed solar energy is reached per unit meter of the absorber, by 2.2.43 heat loss per unit meter is also known. Subtracting 2.2.43 from 2.2.44 gives a net gain of fluid. Since the inlet temperature, outlet temperature and heat capacity of the fluid is known one can find the mass flow rate. By reaching the mass flow rate one can simulate hourly and reach the performance of the solar field.

3 Modelling the Andasol Power Plant

3.1 Brief Overvief of the Andasol Power Station

Andasol Power Station is located in Guadix in the province of Granada. There are three power plants consisting of Andasol I, Andasol II and Andasol III. Andasol I started operation in March 2009 [4], Andasol II in mid-2009 and Andasol III in September 2011. The power plants are identical in construction. Andasol I is the first parabolic trough power plant in Europe moreover it is the first one in the world with thermal storage [16]. Each plant has a nominal capacity of 50 MW_e model here considered is for Andasol I but can be applied for sister plants.

Figure 19: Andasol I, II and III

Each power plant has an aperture area of 510,120 m^2 209,664 reflecting mirrors, consists of 156 collector loop and each loop has 4 Solar Collector Assembly (SCA) unit, each

[4] https://www.power-technology.com/projects/andasolsolarpower/

SCA unit consists of 12 SCE and one SCE has 3 absorber tube in it, so in total one plant has 22,464 absorber tube of Shott PTR-70, 7,488 SCE [17].

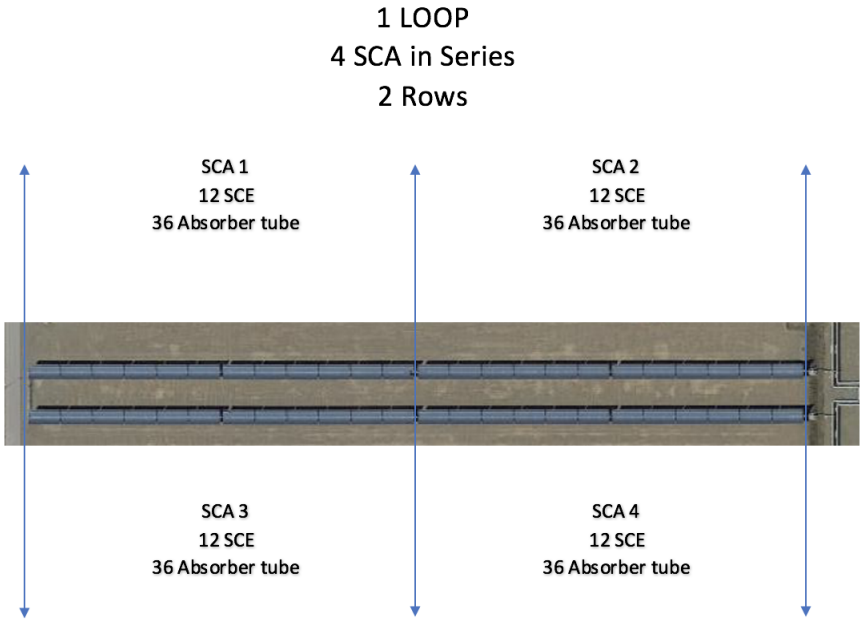

Figure 20: A single loop

Andasol Power Plants have thermal reservoirs where they can store thermal energy with help of two tank indirect molten salt storage. In case of cloudy days or rain and after sunset reservoir can supply 7.5 h of a full load to the steam turbine, where the steam power plant is made up of 50 MW Siemens SST-700 reheat steam turbine [16].

3.2 Annual Performance Modelling of the Andasol Power Plant

3.2.1 The Layout of the Plant

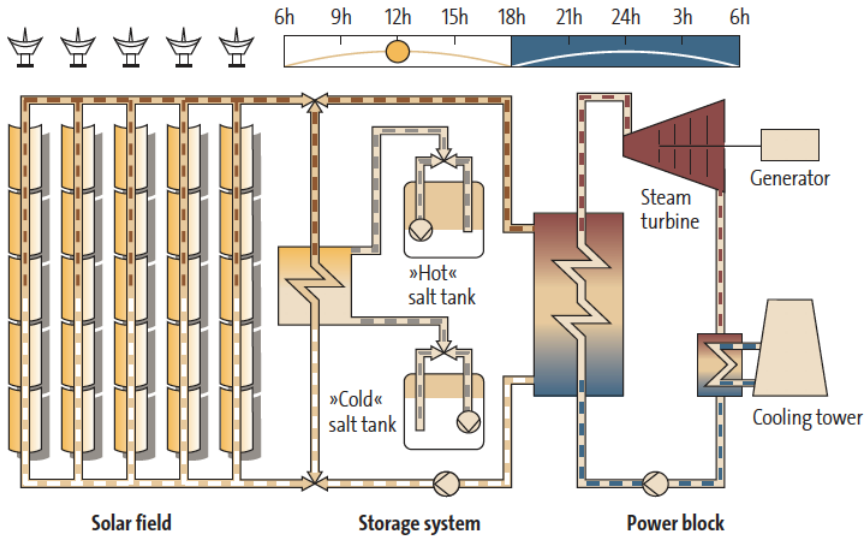

Figure 21: Andasol Power Plant Layout [17]

Andasol Power Plants consists of three main loops, solar field, storage and steam power plant. Sun rays available are directed to absorber tubes by a fraction of 0.7 to 0.8, in absorber pipes circulating fluid is heated from 293 °C to 393 °C .[18] Mass flow rate is controlled through pumps to keep the desired outlet temperature. Then heated thermal fluid is pumped to the heat exchanger between the solar field and power block, the heat of thermal fluid is used to heat up the steam to generate electricity, if available power in thermal fluid is higher than the capacity of steam turbine, part of fluid is diverted into heat exchanger between solar field and storage. Stored energy is used when irradiation is not enough in cloudy or rainy days or during night time for planned electricity production.

3.2.2 Andasol Model

The model should start from the solar field, first one need to reach the radiation, wind speed and temperature data for the Andasol location, latitude is 37.228528 North and longitude is 3.068536 West. There are various databases with subscription fees, thanks

to European Commission one can reach data for any location through their system [5], data is supplied as Typical Meteorological Year where it is a collation of weather data for various years. Hourly values of solar radiation, wind speed, humidity, air pressure is supplied. All of the calculations related with Model is done by MATLAB.

Date & Time	Tamb	ϕ(%)	Horizontal Irr.(W/m^2)	I_b(W/m^2)	Windspeed (m/s)
01/01/2010 08:00:00	6.77	99.94	58	105.24	6.08
01/01/2010 09:00:00	6.90	95.54	233	539.7	6.99
01/01/2010 10:00:00	7.03	91.13	348	537.44	7.90
01/01/2010 11:00:00	7.16	86.73	296	128.62	8.81
01/01/2010 12:00:00	7.17	84.86	462	576.41	8.47
01/01/2010 13:00:00	7.17	82.99	398	397.11	8.13
01/01/2010 14:00:00	7.18	81.12	263	149.82	7.79
01/01/2010 15:00:00	6.74	84.37	235	393.89	6.62
01/01/2010 16:00:00	6.30	87.62	103	350.12	5.45

Table 3: TMY Data

Hourly radiation data is reached; however, as mentioned before solar hour calculation is necessary to calculate angular relations. Equations 2.1.1 to 2.1.7 is used to reach the angle of incidence hour by hour.

[5] http://re.jrc.ec.europa.eu/pvg_tools/en/tools.html#TMY

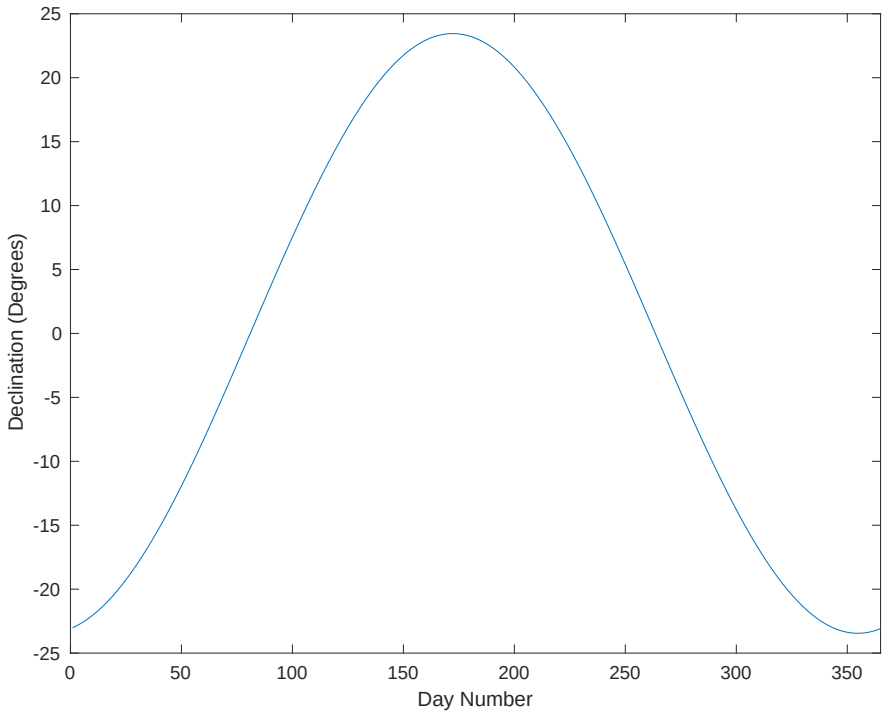

Figure 22: Declination versus Day

In calculating incidence angle declination of the earth is effective, since the position of the specified location varies within time according to the declination, see equation 2.1.5 & 2.1.7.

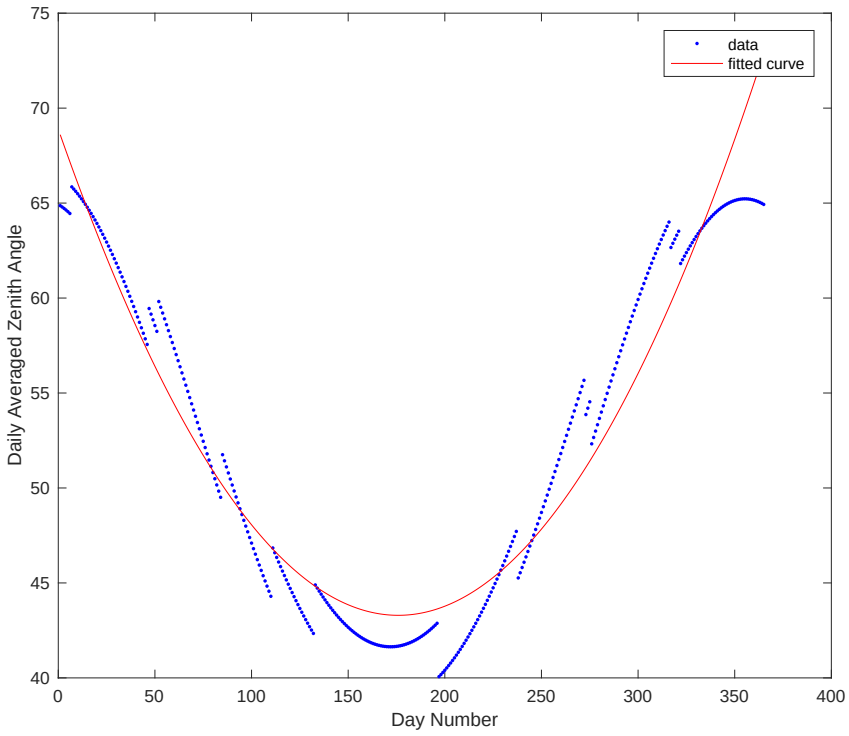

Figure 23: Zenith Angle versus Day

Then the second important parameter here is zenith angle, zenith angle is the angle between the surface normal and sun, which also varies in a year due to declination. Moreover varies in a day by solar time, it is at the minimum when it is solar noon. It becomes minimum for Northern Hemisphere locations 21st of June at solar noon. In Figure 23, zenith angle is shown as daily average where angles higher than 90° is not included in calculation, there are jumps in the graph. Jumps are caused by the algorithm is not taking the zenith angle when it is higher than 90° and than averages it with hour number accordingly. Since incidence angle varies the hours which incidence angle is smaller than 90° varies so a curve is fitted for better visualization. One can easily see that the zenith angle decreases with declination.

Incidence Angle is found per every hour where solar radiation is available. Since continuous North-South axis tracking is adjusted, the maximum incidence angle does not go beyond 10°. Moreover, the incidence angle gets lower when it is summer time. Daily averaged incidence angle is below.

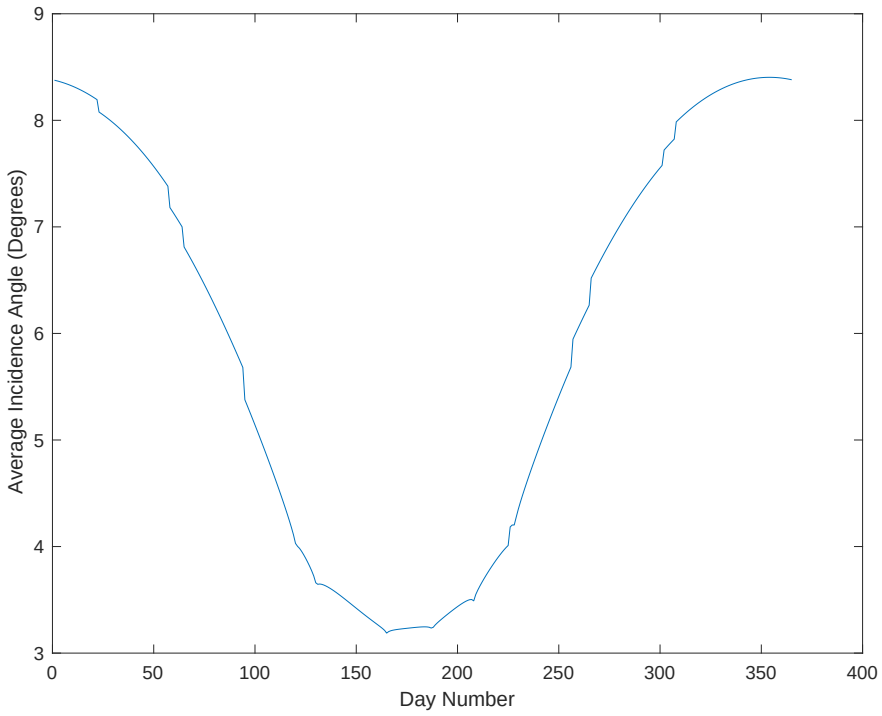

Figure 24: Daily Averaged Incidence Angle

Next thing to model is irradiation available on the solar field, so starting from hourly beam radiation and using 2.1.8 direct radiation on reflecting mirrors is found, and there is a decrease due to optical efficiency η_{opt} :

Optical efficiency is a function of reflectivity, transmissivity, absorptivity and intercept factor [19]:

$r = 0.932$

$\tau = 0.96$

$\alpha = 0.95$

$f_{intercept} = 0.954$

So optical efficiency is $\eta_{opt} = 0.81$. Available solar irradiation is decreased %19 percent when it is on absorber tube, Figure 25 shows the irradiation from the sun to 1 m section of aperture area versus Irradiation on the absorber.

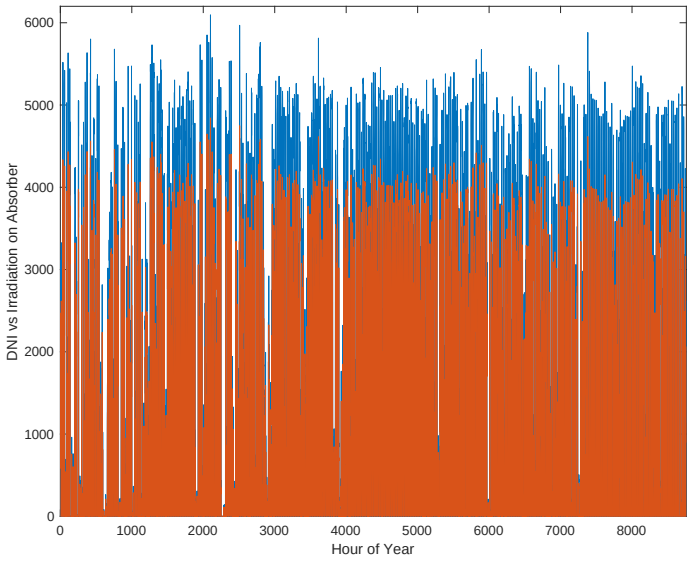

Figure 25: DNI versus Irr. on Absorber

Irradiation available on the surface further faces loss when being transferred to the working fluid, this losses explained in previous chapter and in our model we modeled this loss by correlation coefficients generated by Burkholder and Kutscher. Figure 26, shows the maximum heat possible can be absorbed by the fluid without any constraints.

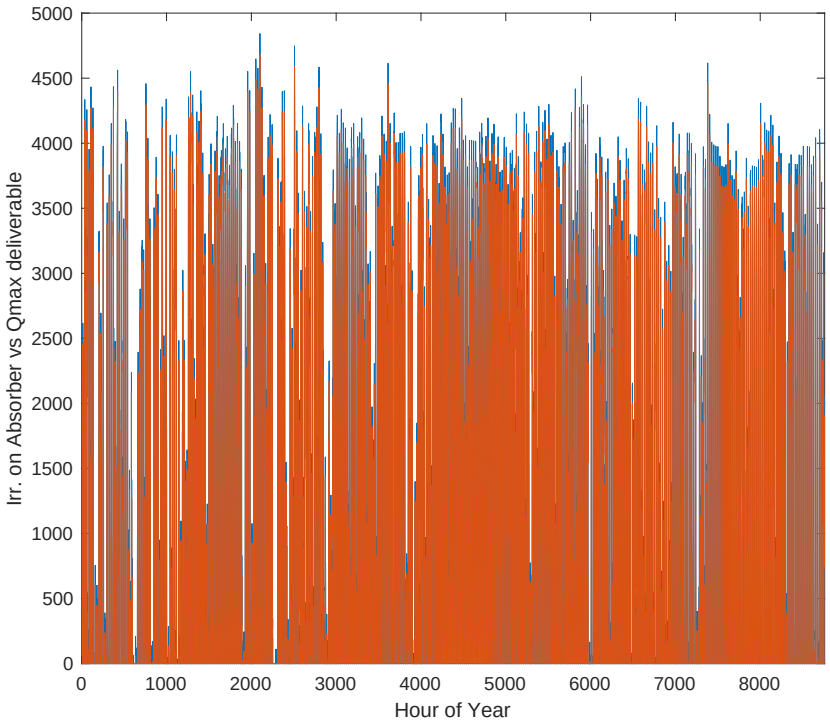

Figure 26: Irr. on Absorber vs Qmax deliverable to fluid

Here we should describe the heat transfer fluid, heat transfer fluid used in power plant is Downtherm A [18], in our model we used different fluid called Therminol VP-1, since it is the one most used in literature because of its available data online, and comparison of the result reached will be more meaningful. Therminol VP-1 is widely used in CSP plants due to its highly stable properties from 12°C to 425 °C. Its properties are supplied by Solutia Company by functions[20].

$$Heat\ Capacity(kJ/kg \cdot K) = 0.002414 \cdot T(^{\circ}C) + 5.9591 \cdot 10^{-6} \cdot T^2(^{\circ}C)...$$

$$-2.9879 \cdot 10^{-8} \cdot T^3(^{\circ}C) + 4.4172 \cdot 10^{-11} \cdot T^4(^{\circ}C) + 1.498 \qquad (3.1)$$

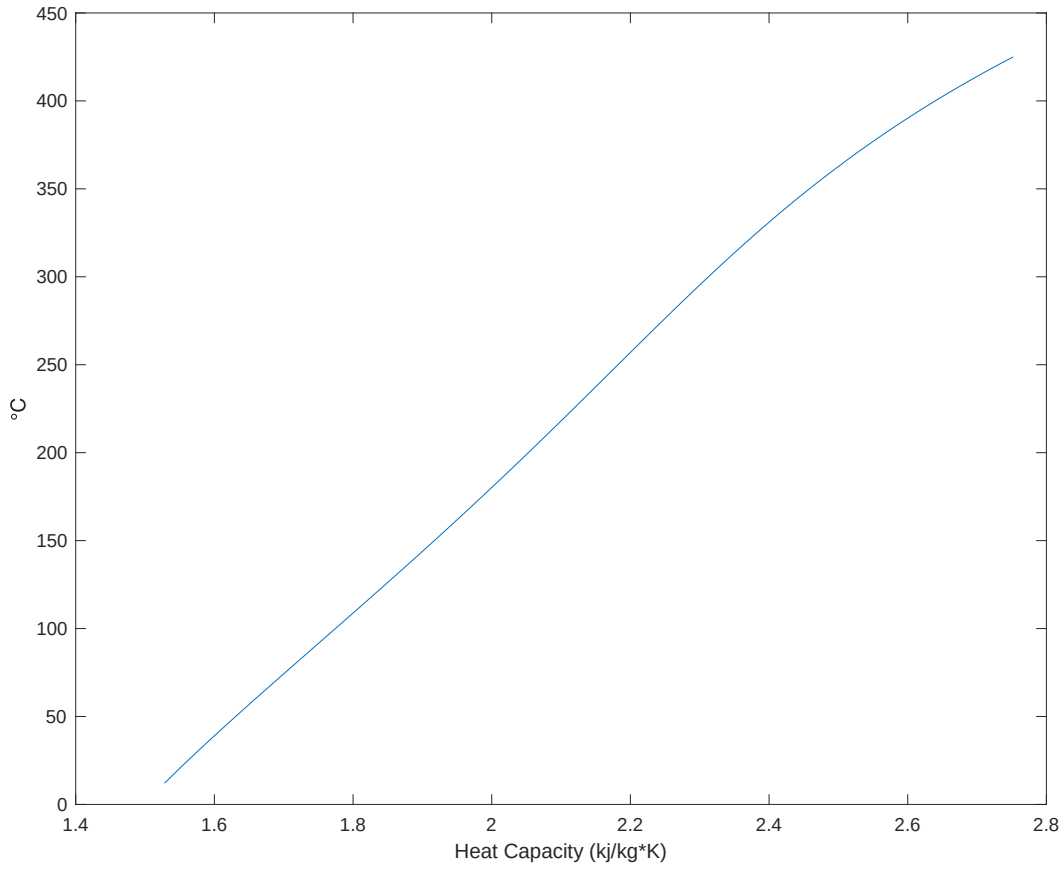

Figure 27: Therminol VP-1 Heat Capacity

All available solar power for absorption is not possible since there are some constraints[19]:

As stated in Llorente's model maximum mass flowrate in one loop can be 7 kg/s, in this thesis same flow rate is used and also the minimum flow rate is assigned as 2 kg/s for Turbulent flow conditions. The maximum thermal power that can be sent to Power Block is 140 MW, and the maximum power that can be sent to storage is 100 MW. Which means when the absorbed power is 240 MW, further absorption by the fluid is not possible so excess energy is not absorbed, by defocusing part of SCA's, it is called dumping.

When we move to Power Block, Power Block is a steam power plant where turbine is 50 MW Siemens SST-700 reheat steam turbine. As explained maximum thermal power deliverable to power block is 140 MW more over minimum is assigned as 19 MW, with heat exchanger efficency $\eta_{exch} = 0.95$. Of course, only a portion of thermal energy can

be converted into electricity and power block efficiency is explained as the following function :

$$\eta_{PB}(P_{thermaltoPB}) = a1 + a2 \cdot exp(\frac{-P_{thermaltoPB}}{a3}) \qquad (3.2)$$

$$a1 = 0.397$$

$$a2 = -0.243$$

$$a3 = 28.23\, MW_{thermal}$$

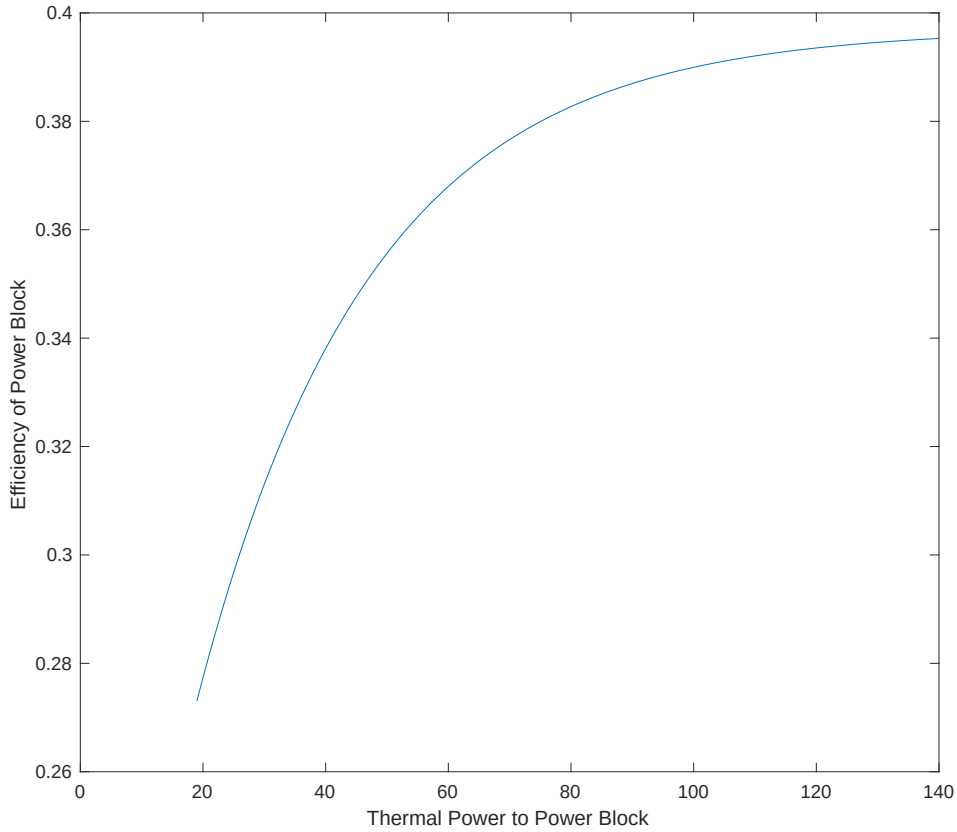

Figure 28: Power Block Efficiency

If the power output from Solar Field exceeds maximum power that can be used in Power Block main advantage of CSP comes out, thermal storage by two tanks (indirect storage). It is said in literature with various sources that storage is 7.5 equivalent hours [19][17],1010 MWh with 28500 tons of molten salt of 60% sodium nitrate and 40% potassium nitrate. As mentioned above maximum thermal power from Solar Field to Storage is 100 MW and the minimum is 21 MW during the charge of storage and while the minimum thermal power discharge from storage to the solar field is 16 MW and the maximum is limited with 124 MW. In this model discharge from storage is assumed to start at 10 a.m. with local time, giving time to solar field pipes heat up and become to steady state and discharge ends at 24 p.m. by this demand hours of a day can be covered by storage.

3.2.3 The Model Validation and the Results

We can reach the radiation data in hourly basis as TMY data, not the actual values, and calculation is made steady state in each every hour. Comparison with actual plant data is not possible in this case but overall efficiency and power output calculation will be made for validation.

$$System\ Efficiency = \frac{Total\ Electricity\ Produced}{Total\ Radiation\ Energy}$$

$$Total\ Electricity\ Produced = \sum \dot{Q}_{toPB} \cdot \eta_{PB}$$

$$Total\ Radiation\ Energy = \sum I_b \cdot Ap \cdot Loop \cdot SCAperloop \cdot SCAlength$$

Ap is aperture area.

$Loop$ is total loop number.

$SCAperloop$ number of SCA per loop.

$SCAlength$ length of an SCA.

Results of	Andasol	SAM Case	MODEL
electricity output(Annual)	180 GWh	174 GWh	171 GWh
System Efficiency(Annual)	15%	N/A	15.6%

The model can be said to be obeying the values of supplied by Solar Millenium [17] and SAM Case Study [16] so validated in a macro manner.

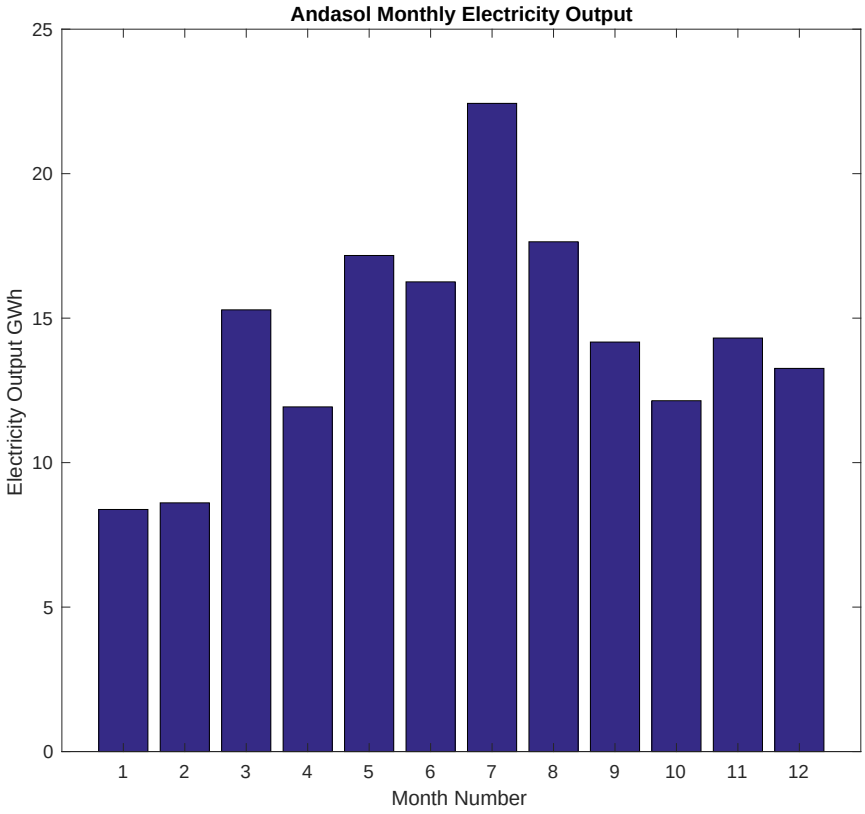

Figure 29: Andasol Monthly Output

Examining Figure 29, Andasol reaches its maximum electricity output as 22.43 GWh in July and minimum in January with 8.38 GWh, distribution of output does not have abnormality as it is increasing towards summer and decreasing towards winter.

Average days of Months are as [10]:

Month	Date
January	17
February	16
March	16
April	15
May	15
June	11
July	17
August	16
September	15
October	15
November	14
December	10

Table 4: Average Days of Months

Results of average days of each month:

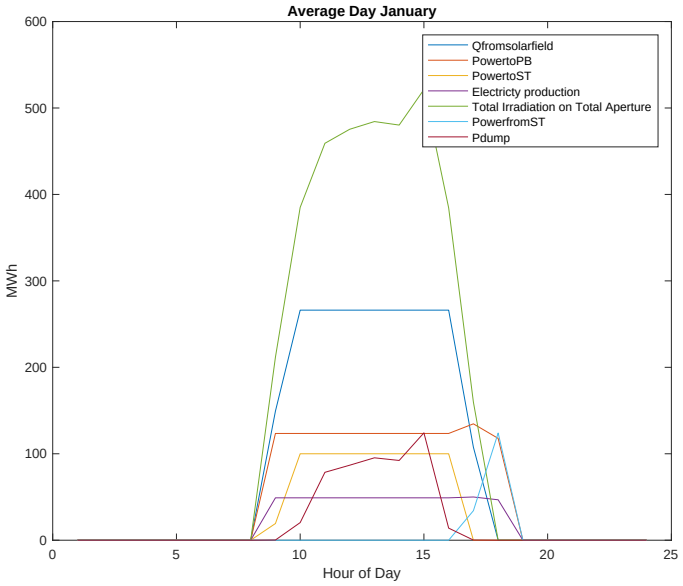

Figure 30: Power Plant on average day of January

As the stated average day of January is 17th in literature; however, in our results, we showed 18th because the radiation data was more smooth with respect to 17th. Solar radiation starts at 8 a.m. and electricity production follows it and there is nearly 8 hours of full capacity electricity production. Moreover, there is dumped power and storage feed starts when radiation is not enough and when there is storage capacity.

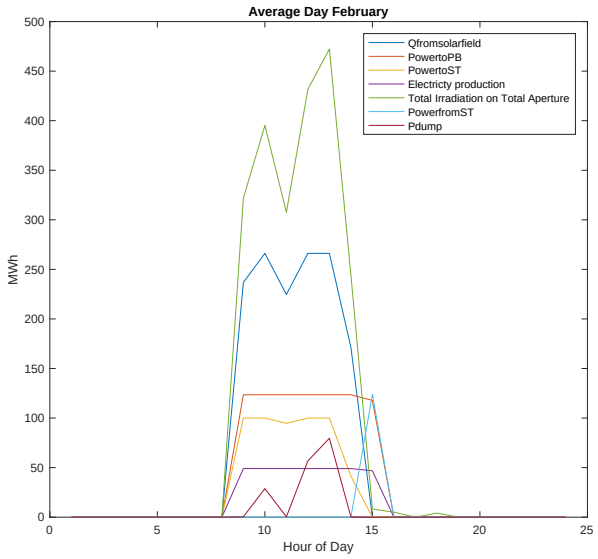

Figure 31: Power Plant on average day of February

Like in January also in February radiation starts at 8 a.m. but nearly 7 hours of full capacity of electricty produced by the generator, due to the low level of irradiation storage feed starts earlier in February and also there is almost no dumped power. Solar irradiation is able to operate Power Block in full capacity only five hours than, storage feed is supplied.

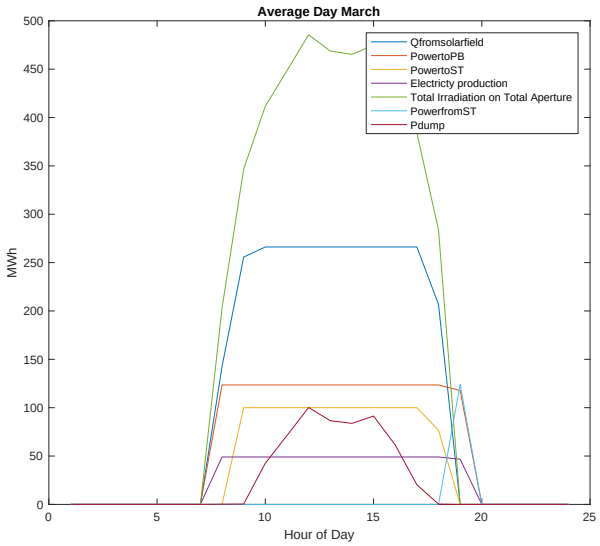

Figure 32: Power Plant on average day of March

On March since sunlight hours starts to increase on the average day of the month, almost 11 hours of full capacity electricity production is observed up to 8 p.m, moreover dumped power increase with respect to average day of February. 10 hours of full capacity production is directly supplied by solar field than storage feed is supplied.

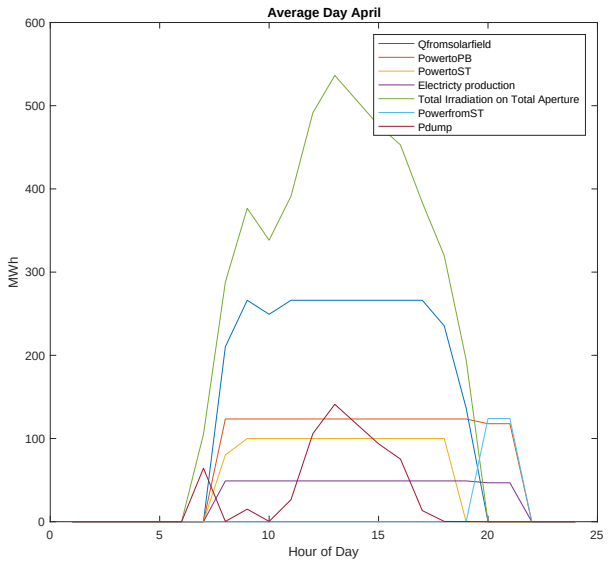

Figure 33: Power Plant on average day of April

On April, daily radiation increases significantly so does the dumped power, also the electricity production hours are from 7 a.m. to 10 p.m. where in total 15 hours of almost full capacity electricity production. The operating hours of the plant shows the potential of CSP plants. 3 hours the Power Block is runned fully by storage.

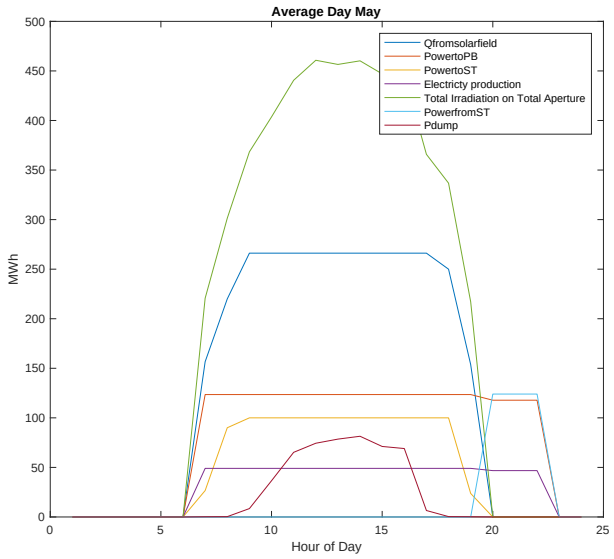

Figure 34: Power Plant on average day of May

On May average day is 15th; Figure 34 belongs to 17th due, May electricity production achieves 16 hours and average radiation achieves higher values on average with respect to previous months. 12 hours of electricity production is fully supplied directly from solar field and 4 hours of supply is done by storage.

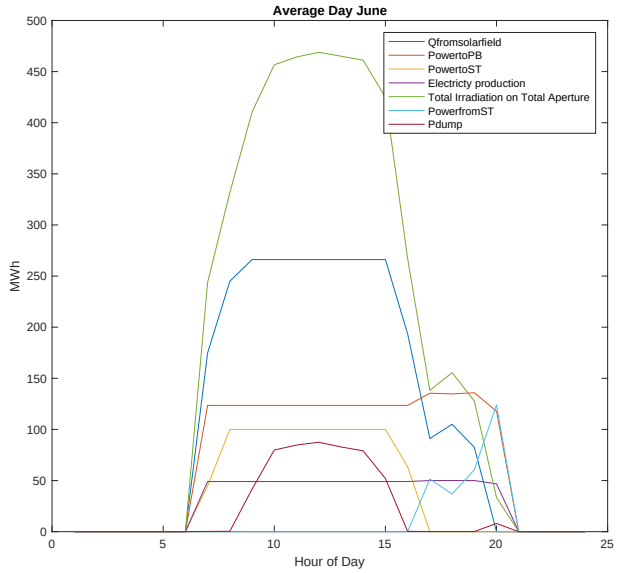

Figure 35: Power Plant on average day of June

June average day is taken as 19th, solar irradiation decreases at 5 p.m. due to the cloudy

or rainy weather. However by storage production continues and 14 hours of production is achieved by the help of storage. We can not generalize that always production on May is higher than production on June, this is only applicable for the average days.

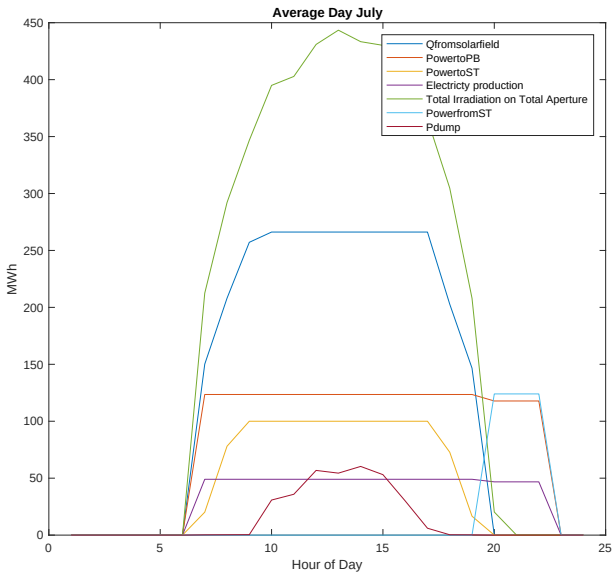

Figure 36: Power Plant on average day of July

July reaches 16 hours of full capacity electricity production, 12 hours of production is supplied directly from the solar field and 4 hours from the storage. Dumped power occurs in solar noon and hours close to the solar noon. Solar field also supplied almost 7 hours at maximum capacity that it can supply to storage.

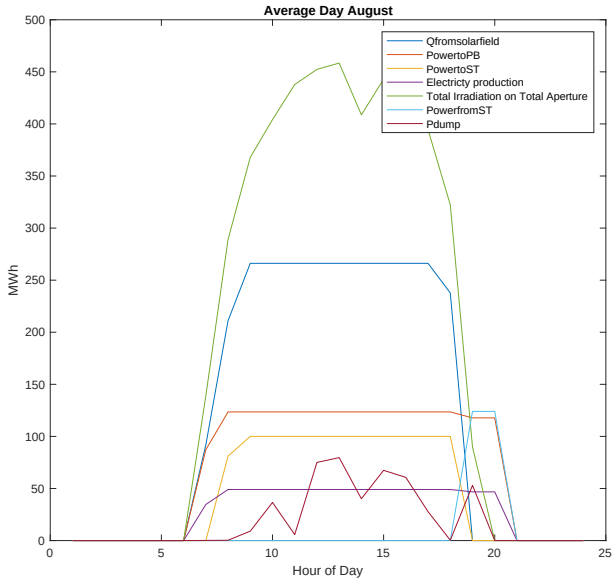

Figure 37: Power Plant on average day of August

August 16th reaches 15 hours of production with 11 directly supplied from the solar field than the rest 4 is supplied from storage. On the average day of August the total production is decreased with respect to the average day of July. Also when we look at the total production of months at Figure 29 "Andasol Monthly Output" total production of July is %20 percent higher than the production on August.

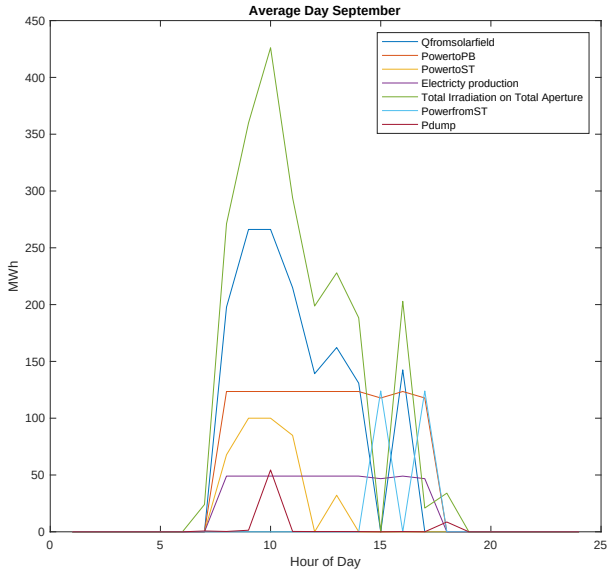

Figure 38: Power Plant on average day of September

On September, there occurs a dramatic decrease in radiation so does at the total electricity production. Electricity is only produced for 8 hours, dumping only occurs one hour and power from solar field to storage is lowest upto now. Monthly output also decreases significantly with respect to August.

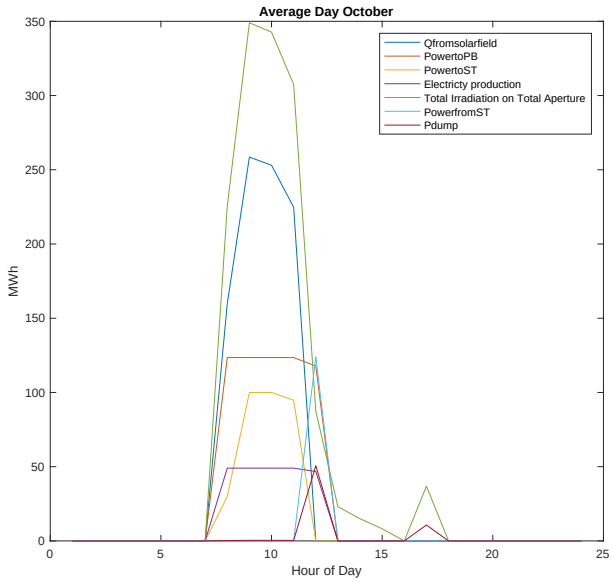

Figure 39: Power Plant on average day of October

On the average day of October electricity production only occurs for five hours, furthermore monthly output decreases with respect to September. It is possible that October is a cloudy and rainy season in the area because of the fact that daily DNI is low but continues until 8 p.m and production ends at 1 p.m.

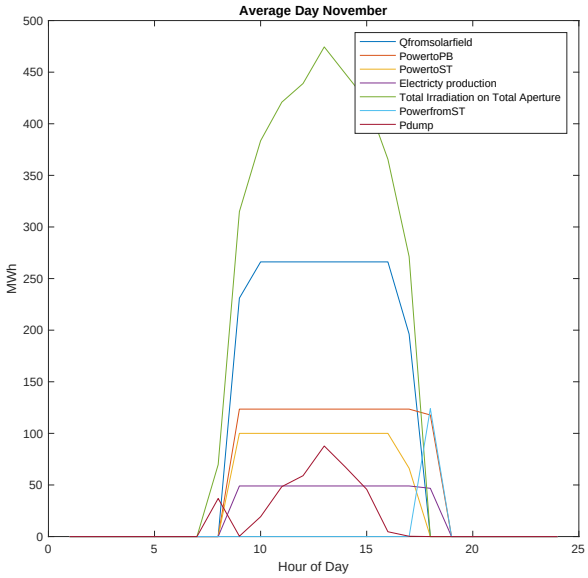

Figure 40: Power Plant on average day of November

November average day shows better results than October as more productive hours occurs and also monthly output is higher thatn september. Dumped power and power supplied to storage increases significantly.

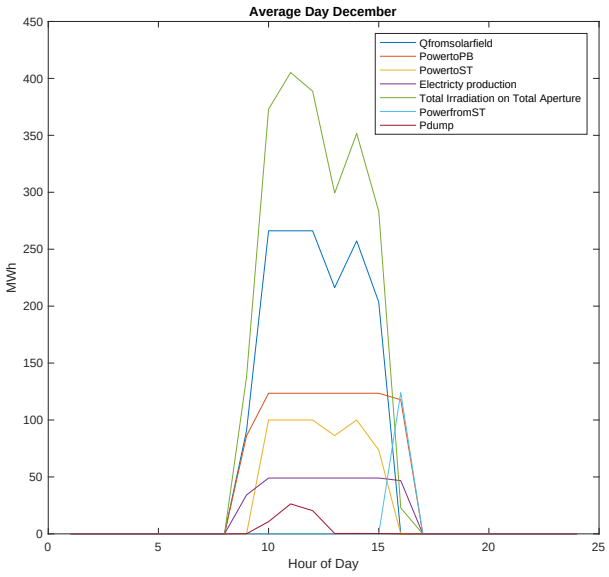

Figure 41: Power Plant on average day of December

December productive hours are only 8, so as a conclusion seasonal dependency of CSP

plants cannot be totally eliminated by storage; however, it can be used for planned dispatch.

4 Case: Turkey

Turkey is geographically located in both continents Asia and Europe, the importance of Anatolia in history should be mentioned briefly. Early civilizations where humans started settling as cities, arose in now in borders of Turkey, Mesopotamia, due to economic activities are related directly with the availability for agriculture and rivers Tigris and Euphrates are perfect for communities to settle around. Then the Ancient Greek cities started to appear, where Anatolia was the crossroads for trade routes as Silk Road. The ancients were able to benefit from the geographical advantages, in this thesis we will focus on benefiting from the solar resources of Anatolia with the help of CSP plants.

First taking look at macro manner for Turkey, Turkey has been showing great development in an economic manner in past years. Neglecting the per capita values, Turkey stands 13th in GDP ranking valuation by PPP [6].

[6]https://data.oecd.org/gdp/gross-domestic-product-gdp.htm#indicator-chart%5D

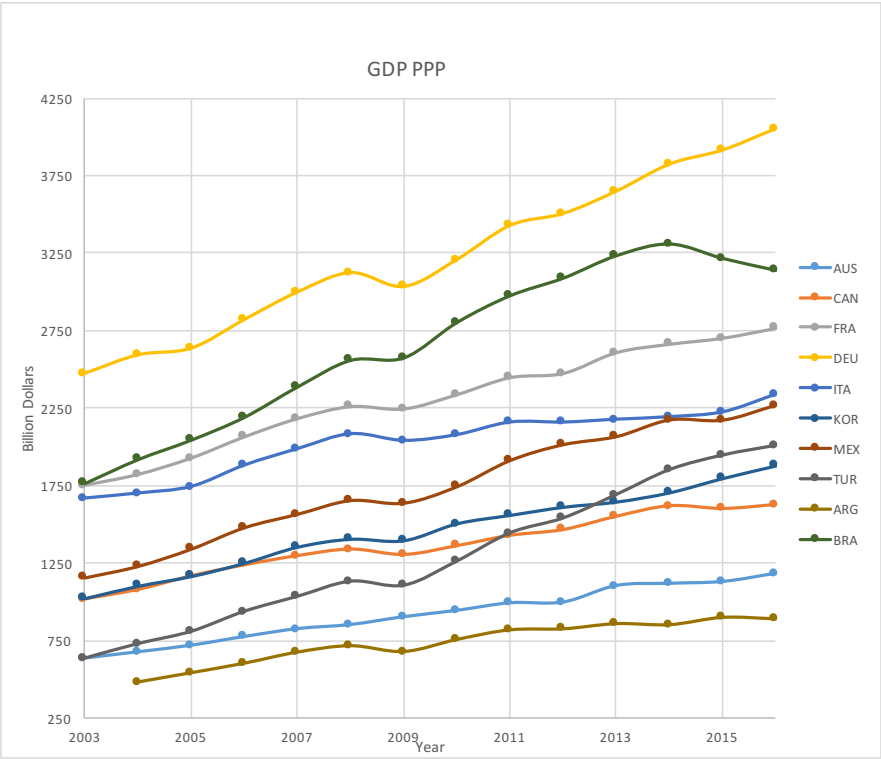

Figure 42: Turkey GDP vs G20

In the Figure 42 PPP applied GDP for some close countries in G20 are examined by data of OECD [7], one thing that we should focus on is the increase of GDP of Turkey in recent years and it surpasses Canada and South Korea in recent years and one can expect Turkey's GDP PPP can surpass Italy and Mexico in upcoming years. Moreover, if we focus on the growth rate, it is significantly higher with those countries as can be seen at the Figure 43 , data is made available by OECD .

[7]https://data.oecd.org/gdp/gross-domestic-product-gdp.htm#indicator-chart

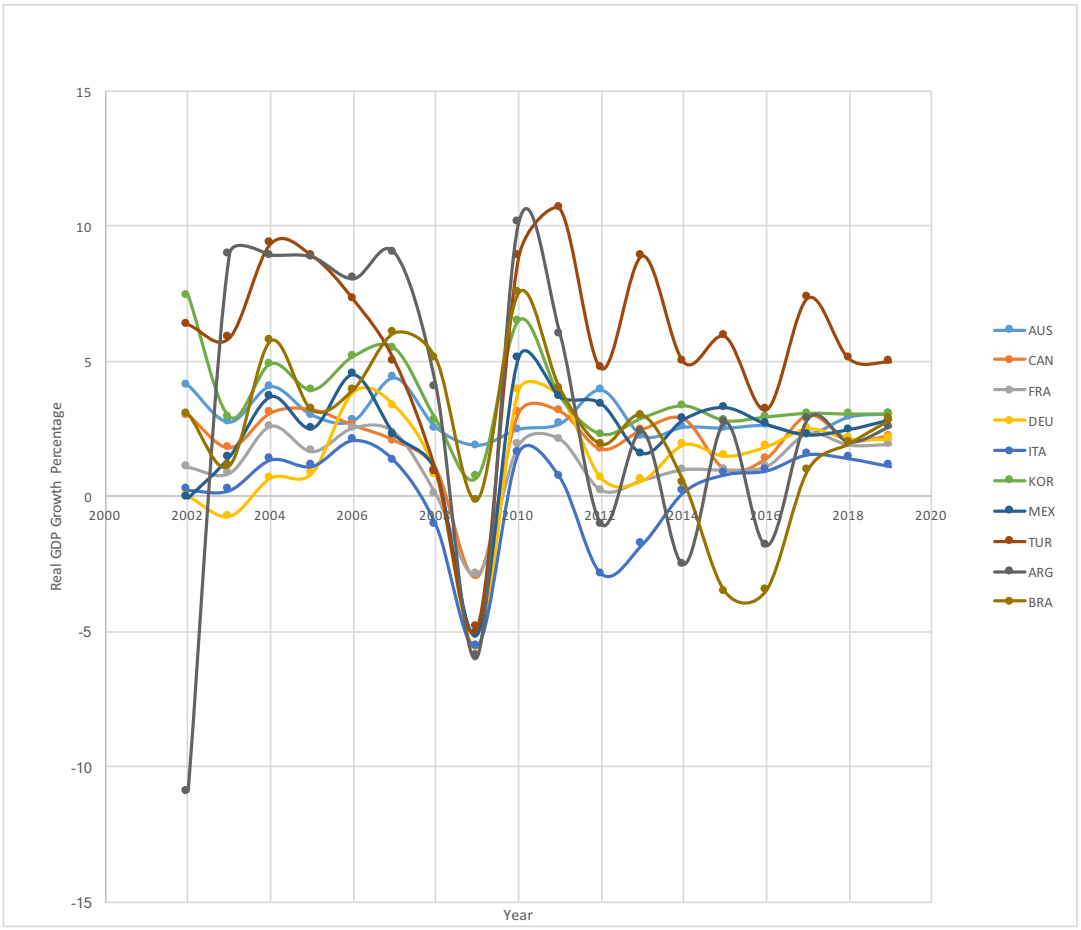

Figure 43: Growth rate of GDP

The higher growth rate comes with a result that vulnerability of the economy is higher with respect to others, in the 2008 crisis Turkey faces one of the highest drop rate of GDP.

The brief description of standing of the Turkish economy is made since there is direct relation with energy consumption and economic output, growing economy means higher demand for Energy. Especially for energy-import-depending countries this link is highly important. When considering 10 hours of blackout hit whole Turkey in 2015, energy security should be another concern. [8]

[8] http://www.hurriyetdailynews.com/explained-how-76-million-people-were-hit-by-turkeys-worst-blackout-since-1999-80442

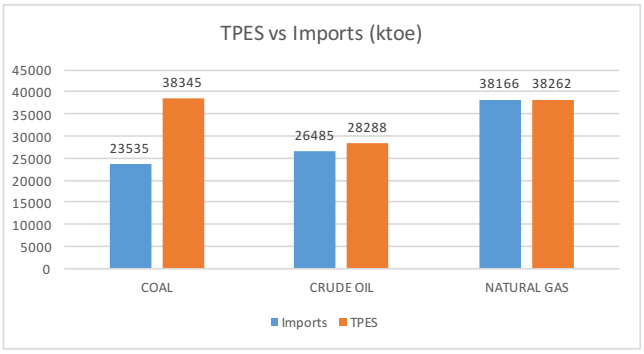

Figure 44: Imports vs TPES

Data gathered from the International Energy Agency [9]Figure 44 shows the dependency of the Turkish Energy sector so the dependency of the Turkish economy on imports.

We should consider electricity production from sources to understand deeply by the data from IEA. [10]

Electricity Production from:	GWh
COAL	92,273
OIL	1,926
GAS	89,227
BIOFUELS	1,635
WASTE	24
NUCLEAR	0
HYDRO	67,231
GEOTHERMAL	4,819
SOLAR PV	1,043
SOLAR THERMAL	0
WIND	15,517
TIDE	0
OTHER	713
TOTAL	274,408

Table 5: Electricity Production by Source

[9]IEAhttps://www.iea.org/statistics/?country=TURKEY&year=2016&category=Key%20indicators&indicator=TPESbySource&mode=chart&categoryBrowse=false&dataTable=BALANCES&showDataTable=true)

[10]https://www.iea.org/statistics/?country=TURKEY&year=2016&category=Key%20indicators&indicator=ElecGenByFuel&mode=chart&categoryBrowse=false&dataTable=ELECTRICITYANDHEAT&showDataTable=true)

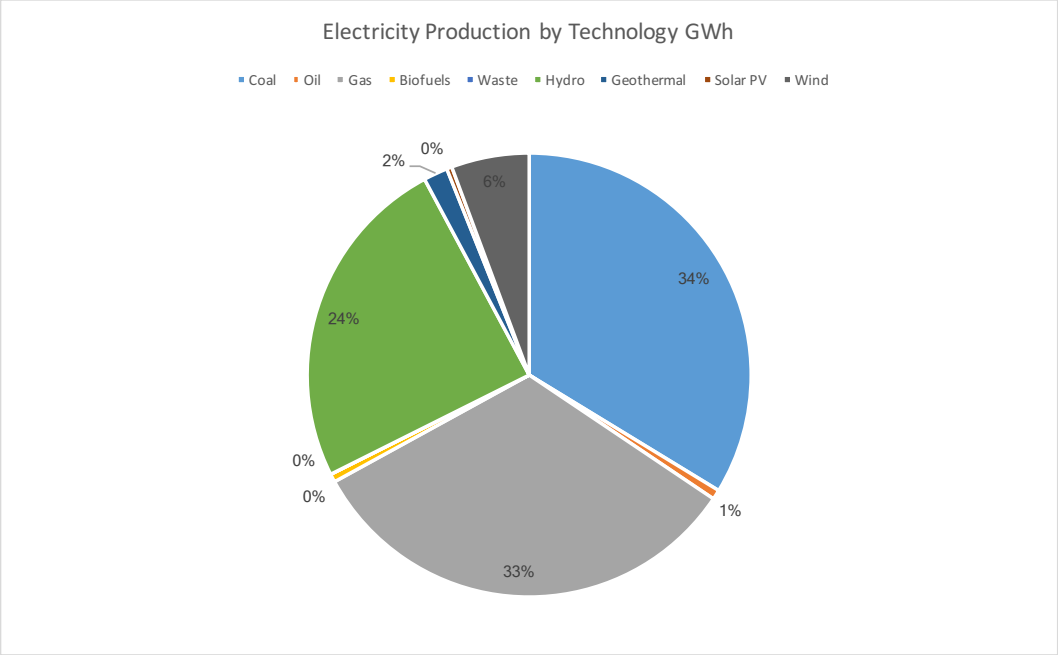

Figure 45: Electricity Generation by Source

As can be seen in Figure 45 and Table 5 big three comes from Coal 34%, Gas 33% and Hydro 24%. First two sources are highly import dependent and Hydro can be affected by rainfall during the year, as in 2014 33% decrease of output[11].

When we consider the licensed power plants under construction in scenario 1 according to the report in TEIAS by the private sector (TEİAŞ RPORU KOY) :

[11]https://www.aa.com.tr/en/energy/renewable/drought-causes-fall-in-turkey-s-hydro-power/12055

Resource	2018	2019	2020	2021	2022	Uncertain date	General Total
Biomass (MW)	25.6	16.1	-	-	-	21.9	63.6
Waste (MW)	-	4.2	-	-	-	-	4.2
Natural Gas (MW)	1,097.2	-	392.8	-	-	3,168,4	4,658.5
Fuel oil (MW)	19.1	-	-	-	-	-	19.1
Solar PV (MW)	-	-	-	-	-	20	20
Hydro (MW)	1,470.8	231.3	922.3	531.1	5.3	1,468	4,628.7
Import Coal (MW)	-	-	-	2,045.5	-	2,270	4,315.5
Geothermal (MW)	149	20.3	3	-	-	-	172.3
Nuclear (MW)	-	-	-	-	-	4,800	4,800
Wind (MW)	193.3	844.6	1,724.2	-	-	643.8	3,405.8
Aspahltites (MW)	-	-	-	-	-	135	135
Coal (MW)	-	-	-	-	-	1,100	1,100
Lignite (MW)	790	-	-	500	-	-	1,290
Total (MW)	3,745	1,116.5	3,042.3	3,076.6	5.3	13,627.1	24,612.6

Table 6: Private Sector Capacity Construction

and than by public sector :

Resource	2018	2019	2020	2021	2022	Uncertain date	General Total
HYDRO (MW)	137.7	1,204.2	548.1	-	-	-	1,890
Total (MW)	137.7	1,204.2	548.1	-	-	-	1,890

Table 7: Public Sector Capacity Construction

and alsor RERAs are in regulation since 2005, Renewable Energy Resource Areas and they have their own legislation [12]. It shows a boom in upcoming years for Solar PV and Wind power plants.

Resource	2018	2019	2020	2021	2022	Total	Unceartain date	General Total
Solar PV (MW)	-	500	500	-	-	1,000	-	1,000
Wind (MW)	-	-	500	500	-	1,000	-	1,000
Total (MW)	-	500	1000	500	-	2,000	-	2,000

Table 8: RERA Construction

From the tables above it can be said that the general trend is again between Natural Gas, Coal, Hydro and first Nuclear Power Plant of Turkey is under construction, although some actions are taken with RERAs it can not be said that Turkey is soon changing

[12] http://www.cakmak.av.tr/articles/Power/107724240_3.pdf

its energy mix from conventional to Renewable. We mentioned the drawback of Hydro plants, as in 2014 due to the drought and decreased the power output at least 33%, and when considering about PV and Wind without storage, planned dispatch is not fully possible.

To unleash import dependency of the Turkish Energy sector, directing new capacity formation to its own resources is the only way, investment on Hydro, Wind and PV is a way out from high dependency. However, CSP will result in planned dispatch so continuous investment on new CSP plants and supplied with other RERAs may unleash totally in long-term perspective.

In his article Bülent Aksoy [22] , showed the map of annual global solar irradiation of Turkey, based on 22 years average NASA data.

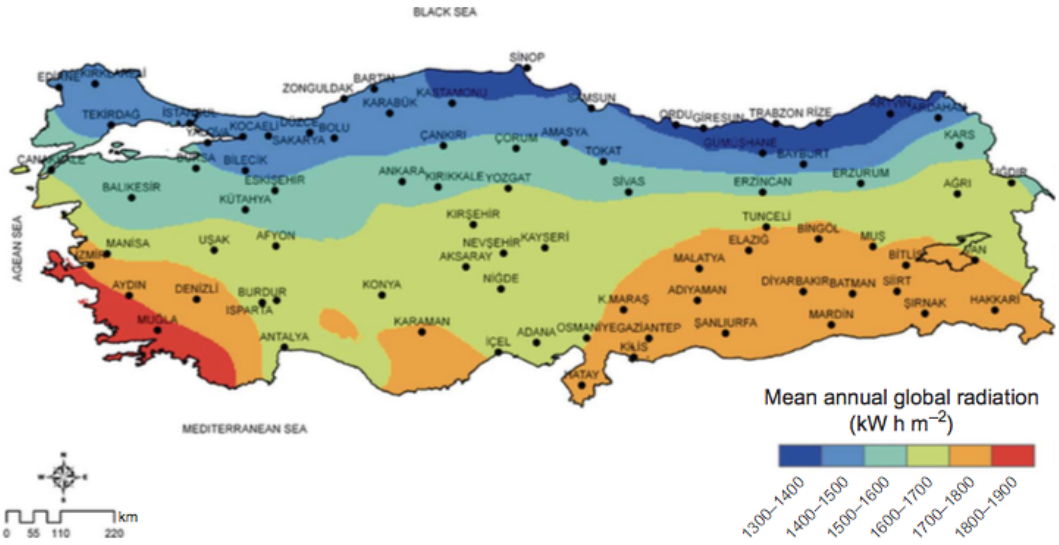

Figure 46: Turkey Solar Irradiation Map

In the northern part of Turkey, solar irradiation is respectively low and it is inreasing with moving to the south. Lands in the south-west of Turkey is highly touristic, centre-south and south-east part of Turkey consists of wasted lands, so in this thesis, we should focus on either mid-south part or south-east part. However, one main problem in south-east part is the conflict in Syria, due to the extreme length of the border with Syria the border cities are eliminated from consideration. Internal parts of south-east suffer from internal conflicts of Turkey and the most feasible location is the central part of south, where also 1 GW of RERA PV is under construction.

Another solar map is published in the article of Kaygusuz [23]:

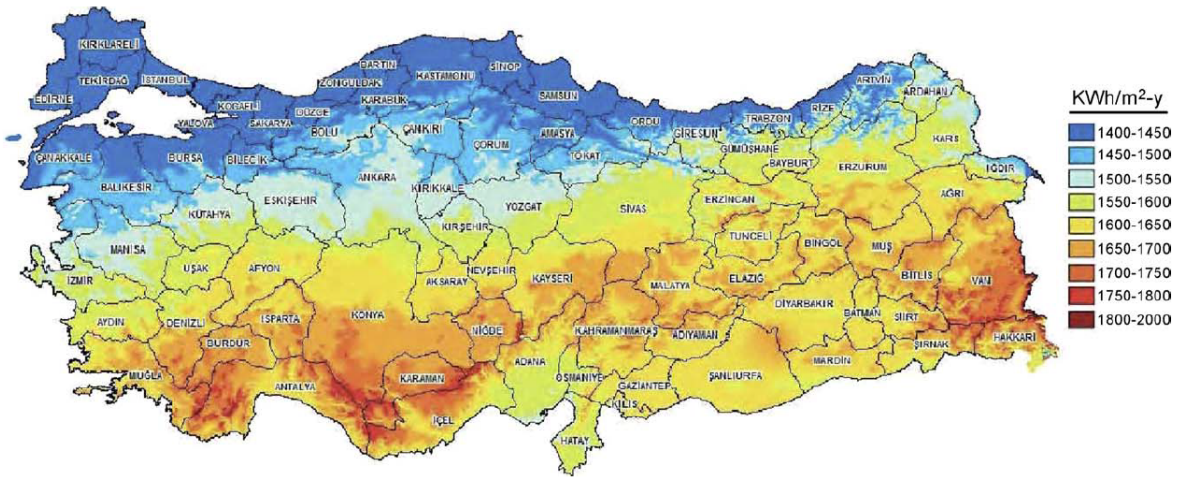

Figure 47: Turkey Solar Irradiation Map 2

In this map, it is seen that centre-south part receives the highest radiation. Moreover, in the article of Kaygusuz, he suggested constructing a plant in southern Konya, where RERA is closely located. Furthermore, in this thesis our validated model will be simulated in that area.

The location chosen is Karapınar/Konya, 37.60 North and 33.49 East. the slope of the land is suitable for plant construction. Moreover no dense settling is present in the area.

Figure 48: Karapınar

4.1 The Model Results for Turkey

The model developed in this thesis is simulated in location described above.

Indicator	Model Result Karapınar	Model Result Andasol
Electricity Output GWh (Annual)	187.14	171.59
Efficiency (Annual)	16.97%	15.63%

Yearly output of a single hypothetical twin power plant output which could be constructed in Karapınar will result in both higher efficiency and higher electricity output compared with real Andasol Power plant.

Monthly comparison of Andasol and hypothetical twin plant in Karapınar output will be showed below :

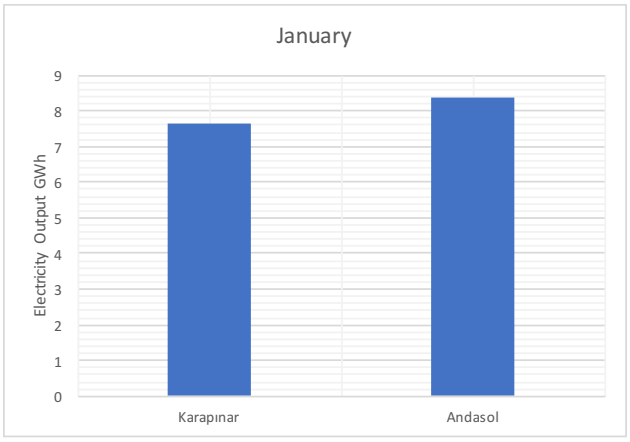

Figure 49: January Comparison

In January Andasol Power Plant has slightly higher output, in that zone of Turkey winter time is coercive, heat loss to ambient and cloudy day increases.

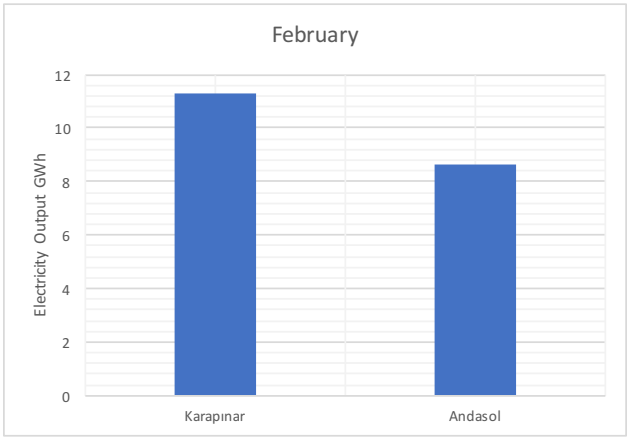

Figure 50: February Comparison

In February hypothetical twin plant has perceptibly higher output than Andasol; however both plants have really low output with respect to other months.

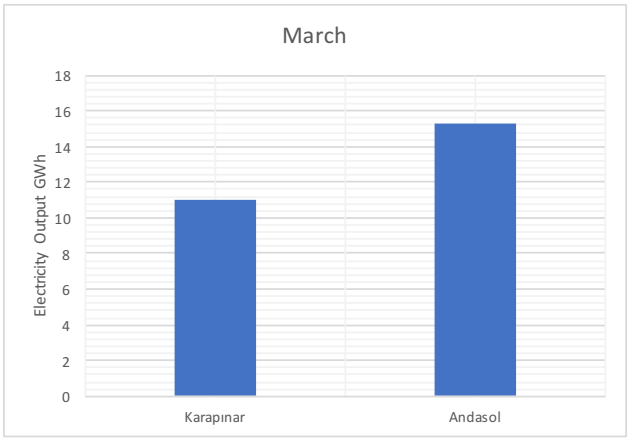

Figure 51: March Comparison

In March Andasol has almost 4 GWh higher output than the hypothetical plant, this is due to again cloudy days and heat loss to ambient.

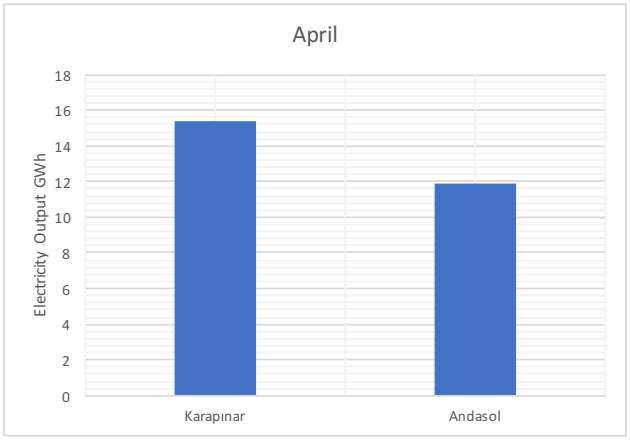

Figure 52: April Comparison

In April output of hypothetical twin plant in Karapınar overcomes the output from Andasol and holds it until October. The zone Karapınar has desert climate and this results in higher variation of output with respect to Andasol in seasons.

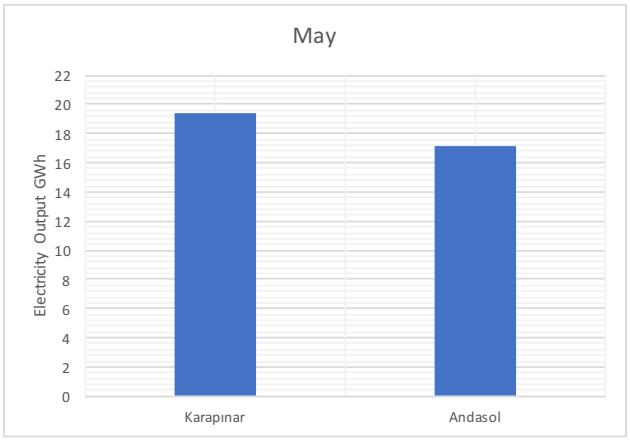

Figure 53: May Comparison

In May there is a 10% difference of output where Karapınar's output is higher, Konya zone of Turkey summer arrives in the middle of May.

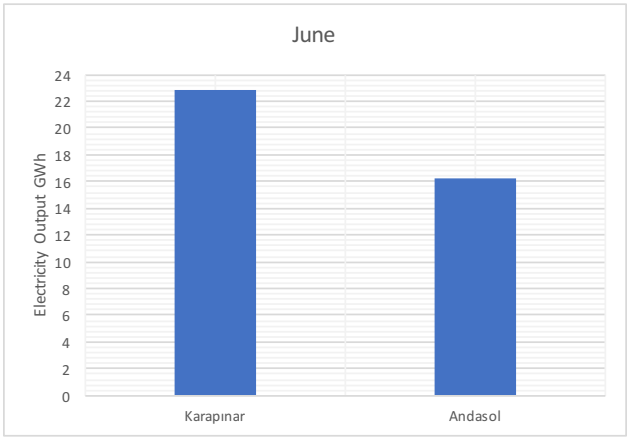

Figure 54: June Comparison

In June the output of Karapınar reaches 1.5 times Andasol output, summer arrived to Konya and extreme suny days occurs.

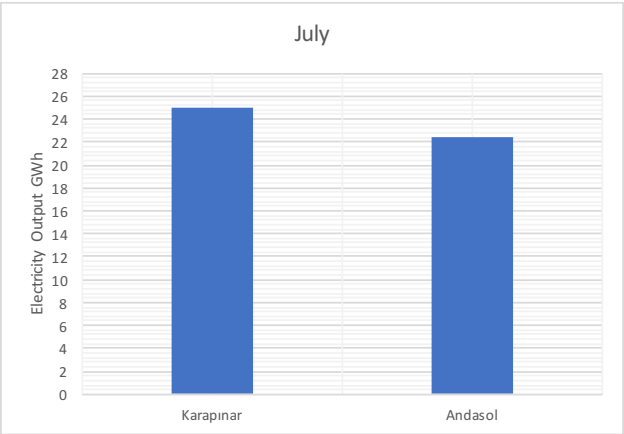

Figure 55: July Comparison

Karapınar's leadership in output continues and both plants output increases, this is the highest output achieved in monthly perspective for both of the plants.

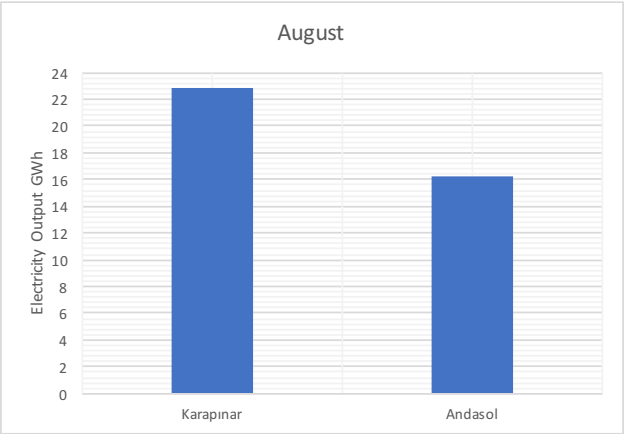

Figure 56: August Comparison

In August difference increases with respect to July, Karapınar's output decrease with respect to July however decrease in Andasol is more significant than Karapınar.

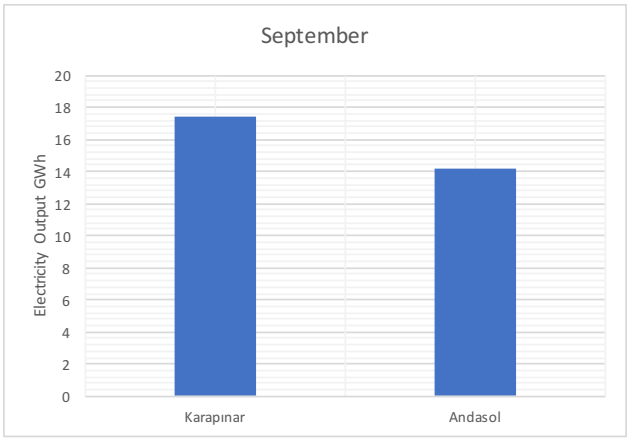

Figure 57: September Comparison

In September Karapınar remains at higher output; however difference with respect to August is decreases since.

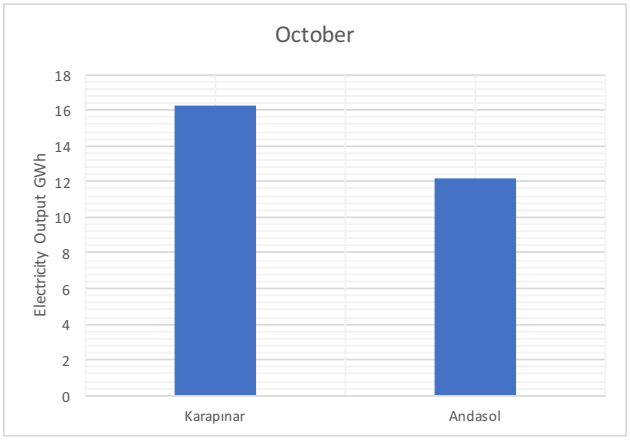

Figure 58: October Comparison

In October Karapınar remains at higher output and difference remains almost constant, there is 2 GWh decrease for each of them from previous month.

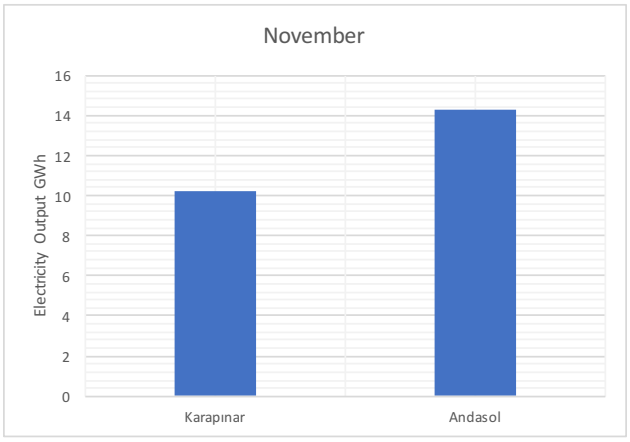

Figure 59: November Comparison

In November winter hits Karapınar and there occurs 4 GWh difference and Andasol takes the leadership.

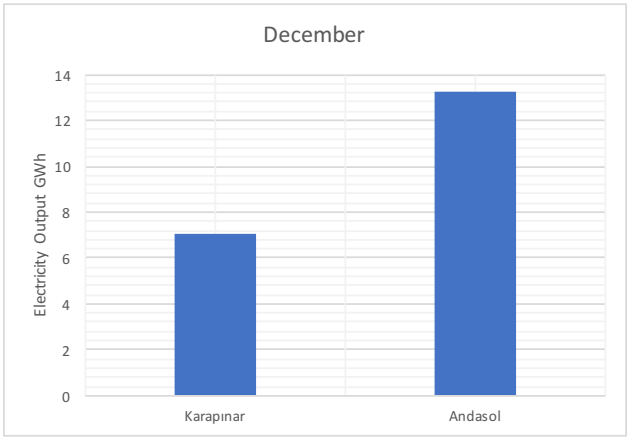

Figure 60: December Comparison

In December difference dramatically increases. However when considering the annual value hypothetical plant in Karapınar has output 16 GWh higher than Andasol, almost 10% higher output in annual value which shows the potential.

5 Conclusion

In this thesis, Parabolic Trough type of Concentrated Solar Power technology is modelled on and simulation of it performed on MATLAB for the Andasol-1 power plant which is located in Guadix/Granada in Spain which is the first Parabolic Trough type plant with thermal storage in Europe. The model results are validated according to real performance output of the plant and a simulation of the plant.

Turkey, its economy and its energy sector are investigated. Key findings are its import-dependent energy sector and high GDP growth rate. Since the import-dependency for energy is an obstacle for sustainable growth of GDP a suggestion for returning to its own renewable resources brought in the discussion. The developed model is used for a hypothetical plant similar with Andasol-1 which is located in the southern part of Turkey. The results were satisfactory, higher annual output and higher annual efficiency with respect to real commercial Andasol-1 plant.

The achieved result from thesis strengthens the report made by IEA [3] that Turkey will head for CSP and becomes an electricity importer to Europe up to 2050. To sum up, an import-dependent country may be self-sufficient and even an importer with innovative investments. As future work, other types of Concentrated Solar Power technology can be compared with cost and output manner for Turkey.

References

[1] "World Energy Resources: Solar" Available: https://www.worldenergy.org/wp-content/uploads/2013/10/WER_2013_8_Solar_revised.pdf [Accessed 18-October-2018]

[2] "World Energy Resources: Solar" Available: https://www.worldenergy.org/wp-content/uploads/2017/03/WEResources_Solar_2016.pdf [Accessed 12-October-2018]

[3] "Technology Roadmap Concentrating Solar Power" Available: https://www.iea.org/publications/freepublications/publication/csp_roadmap.pdf [Accessed 21-October-2018]

[4] Schiel, W., & Keck, T. (2012). Parabolic dish concentrating solar power (CSP) systems. In Concentrating Solar Power Technology (pp. 284-322).

[5] Available: https://www.sbp.de/en/project/10-kw-dishstirling-eurodish-testing-carrier/ [Accessed 16-November-2018]

[6] "Global Review of Solar Tower Technology" Available: http://www.seriius.org/pdfs/global-review-solar-tower-technology.pdf [Accessed 12-September-2018]

[7] Available: https://www.solarreserve.com/en/global-projects/csp/crescent-dunes [Accessed 12-October-2018]

[8] Günther, M. (2016). Advanced CSP Teaching Materials: Chapter 6 Linear Fresnel Technology. EnerMENA, DLR, accessed in, 14(04).

[9] Available: http://www.puertoerrado2.com [Accessed 17-November-2018]

[10] Duffie, J. A., & Beckman, W. A. (2013). Solar engineering of thermal processes. John Wiley & Sons. (page 9-21, page86)

[11] Sudhakar, K., & Bishoyi, D. (2017). Modeling and performance simulation of 100 MW LFR based solar thermal power plant in Udaipur India. Resource-Efficient Technologies, (4), 365-377.

[12] Giostri, A. (2014). Transient effects in linear concentrating solar thermal power plant (Doctoral dissertation, Italy).

[13] Yılmaz, İ. H., & Söylemez, M. S. (2014). Thermo-mathematical modeling of parabolic trough collector. Energy Conversion and Management, 88, 768-784.

[14] Bergman, T. L., Incropera, F. P., DeWitt, D. P., & Lavine, A. S. (2011). Fundamentals of heat and mass transfer. John Wiley & Sons, 517-538

[15] Burkholder, F., & Kutscher, C. F. (2009). Heat loss testing of Schott's 2008 PTR70 parabolic trough receiver (pp. 1-58). Golden, US: National Renewable Energy Laboratory

[16] "System Advisor Model Case Study :Andasol-1" Available: https://sam.nrel.gov/sites/default/files/content/case_studies/sam_case_csp_physical_trough_andasol-1_2013-1-15.pdf [Accessed 12-July-2018]

[17] "The Parabolic Trough Plants Andasol 1 to 3"Available: http://www.solarmillennium.de/Archives/Technology/References_and_Projects/ Andasol__Spain_/The_Construction_of_the_Andasol_Power_Plants_, lang2,109,155.html [Accessed 4-June-2018]

[18] Österholm, R., & Pålsson, J. (2014, March). Dynamic modelling of a parabolic trough solar power plant. In Proceedings of the 10 th International Modelica Conference; March 10-12; 2014; Lund; Sweden (No. 96, pp. 1057-1066). Linköping University Electronic Press.

[19] García, I. L., Álvarez, J. L., & Blanco, D. (2011). Performance model for parabolic trough solar thermal power plants with thermal storage: Comparison to operating plant data. Solar Energy, 85(10), 2443-2460.

[20] "Therminol VP-1" http://twt.mpei.ac.ru/tthb/hedh/htf-vp1.pdf [Accessed 23-July-2018]

[21] "Türkiye Elektrik Enerjisi 5 yıllık Üretim Kapasite Projeksiyonu" Available: https://www.teias.gov.tr/sites/default/files/2017-12/KapasiteProjeksiyonu2017ağustos.pdf [Accessed 14-September-2018]

[22] Aksoy, B. (2011). Solar radiation over Turkey and its analysis. International journal of remote sensing, 32(21), 6261-6272.

[23] Kaygusuz, K. (2011). Prospect of concentrating solar power in Turkey: the sustainable future. Renewable and Sustainable Energy Reviews, 15(1), 808-814.